Comparing and contrasting white matter disorders: a neuropathological approach to pathophysiology

Bugiani, M.

2015

document version
Publisher's PDF, also known as Version of record

3.2

Brain white matter oedema due to ClC-2 chloride channel deficiency: an observational analytical study

M Bugiani*, C Depienne*, C Dupuits, D Galanaud, V Touitou, N Postma, C van Berkel, E Polder, E Tollard, F Darios, A Brice, CE de Die-Smulders, JS Vles, A Vanderver, G Uziel, C Yalcinkaya, SG Frints, VM Kalscheuer, J Klooster, M Kamermans, TEM Abbink, NI Wolf, F Sedel** and MS van der Knaap** (*shared first authors; **shared last authors)

Lancet Neurol 2013;12:659-668

Summary

Background. Mutant mouse models suggest that the chloride channel ClC-2 has functions in ion and water homoeostasis, but this has not been confirmed in human beings. We aimed to define novel disorders characterised by distinct patterns of MRI abnormalities in patients with leukoencephalopathies of unknown origin, and to identify the genes mutated in these disorders. We were specifically interested in leukoencephalopathies characterised by white matter oedema, suggesting a defect in ion and water homoeostasis.

Methods. In this observational analytical study, we recruited patients with leukoencephalopathies characterised by MRI signal abnormalities in the posterior limbs of the internal capsules, midbrain cerebral peduncles, and middle cerebellar peduncles from our databases of patients with leukoencephalopathies of unknown origin. We used exome sequencing to identify the gene involved. We screened the candidate gene in additional patients by Sanger sequencing and mRNA analysis, and investigated the functional effects of the mutations. We assessed the localisation of ClC-2 with immunohistochemistry and electron microscopy in post-mortem human brains of individuals without neurological disorders.

Findings. Seven patients met our inclusion criteria, three with adult-onset disease and four with childhood-onset disease. We identified homozygous or compound-heterozygous mutations in *CLCN2* in three adult and three paediatric patients. We found evidence that the *CLCN2* mutations result in loss of function of ClC-2. The remaining paediatric patient had an X-linked family history and a mutation in *GJB1*, encoding connexin 32. Clinical features were variable and included cerebellar ataxia, spasticity, chorioretinopathy with visual field defects, optic neuropathy, cognitive defects, and headaches. MRI showed restricted diffusion suggesting myelin vacuolation that was confined to the specified white matter structures in adult patients, and more diffusely involved the brain white matter in paediatric patients. We detected ClC-2 in all components of the panglial syncytium, enriched in astrocytic endfeet at the perivascular basal lamina, in the glia limitans, and in ependymal cells.

Interpretation. Our observations substantiate the concept that ClC-2 is involved in brain ion and water homoeostasis. Autosomal-recessive *CLCN2* mutations cause a leukoencephalopathy that belongs to an emerging group of disorders affecting brain ion and water homoeostasis and characterised by intramyelinic oedema.

Introduction

ClC-2 is a chloride channel that is almost ubiquitously expressed in the human body (Planells-Cases & Jentsch, 2009). It is present in plasma membranes and is activated by hyperpolarisation, acidic extracellular pH, and osmotic cell swelling (Planells-Cases & Jentsch, 2009; Thiemann et al., 1992; Grunder et al., 1992; Jordt & Jentsch, 1997). Its functions in human physiology are a matter of debate. Roles in gastric acid secretion, lung development and function, and nephronogenesis have been suggested, but not confirmed (Planells-Cases & Jentsch, 2009; Bosl et al., 2001). Information about the localisation of ClC-2 within the brain comes from rodent studies, which have detected ClC-2 in oligodendrocytes, astrocytes (especially in endfeet), and pyramidal and non-pyramidal neurons in the hippocampus (Blanz et al., 2007; Sik et al., 2000). Evidence suggests that ClC-2 modulates postsynaptic responses to GABA by affecting intracellular chloride concentration in neurons (Smith et al., 1995) and that ClC-2 regulates neuronal excitability (Rinke et al., 2010; Ratte & Prescott, 2011), but the physiological relevance of these findings has not been confirmed.

Physiological roles of proteins can be gleaned from diseases caused by mutations in their genes. No human disease has been unequivocally related to mutations in *CLCN2,* the gene encoding ClC-2. Heterozygous mutations in *CLCN2* were described as a cause of idiopathic generalised epilepsies (D'Agostino et al., 2004; Stogmann et al., 2006; Everett et al., 2007; Saint-Martin et al, 2009; Combi et al., 2009; Kleefuss-Lie et al., 2009; Haug et al., 2009), but this finding was later refuted (Planells-Cases & Jentsch, 2009; Niemeyer et al., 2010) and the original paper was retracted (Haug et al., 2009). Because mutant mice without functional ClC-2 have a leukoencephalopathy with intramyelinic oedema (Bosl et al., 2001; Blanz et al., 2007; Edwards et al., 2010), ClC-2 was proposed to have a role in brain ion and water homoeostasis (Bosl et al., 2001; Blanz et al., 2007); however, this hypothesis has not been confirmed in human beings. A known human disorder characterised by intramyelinic oedema is megalencephalic leukoencephalopathy with subcortical cysts (van der Knaap et al., 1995, 1996 & 2012). Mutations in *MLC1* have been identified in 75% of patients with this disorder (Leegwater et al., 2001; van der Knaap et al., 2010). No mutations in *CLCN2* were reported in the patients without *MLC1* mutations (Sheper et al., 2010). Recently, mutations in *HEPACAM* (also called *GLIALCAM*), which encodes the glial cell adhesion molecule (GlialCAM) -a putative auxiliary subunit of both ClC-2 and MLC1 (Lopez-Hernandez et al., 2011; Jeworutzki et al., 2012)- were identified in patients without *MLC1* mutations (Lopez-Hernandez et al., 2011).

We aimed to study patients with leukoencephalopathies of unknown origin to define novel disorders characterised by distinct patterns of MRI abnormalities (van der Knaap et al., 1999) and identify the mutated genes. We were specifically interested in leukoencephalopathies with MRI evidence of intramyelinic oedema. When we identified *CLCN2* mutations in a group of such patients, we sought further evidence for ClC-2's function in human physiology.

Methods

Study design and patients

In this observational analytical study, we used MRI criteria to recruit adult and paediatric patients from the Amsterdam and Paris leukoencephalopathy databases containing MRI images of patients with leukoencephalopathies of unknown origin submitted from all over the world. Patients with prominent signal abnormalities in the middle cerebellar peduncles, midbrain cerebral peduncles, and posterior limbs of the internal capsules were included in the study.

We studied the MRI results of each patient and scored the appearance and distribution of signal abnormalities. We assessed apparent diffusion coefficient (ADC) values in areas of abnormal signal. Signal intensity on T2-weighted and T1-weighted images and ADC values provide information on tissue microstructure. High ADC values indicate large water spaces; low ADC values indicate small water spaces. Because the study was multi-institutional, MRIs were done with different pulse sequences on machines from different vendors. Therefore, we used a robust cutoff ADC value of 60×10^{-5} mm^2/s, below which the diffusion was considered to be restricted. Subtle diffusion restriction could, therefore, have been missed.

We obtained approval from the institutional review boards of the participating centres in Paris and Amsterdam (Hôpital Pitié-Salpêtrière and VU University Medical Centre) and informed consent from patients and their families.

Procedures

Exome sequencing was undertaken in the three patients with adult-onset disease under the assumption that these patients had one disease with autosomal recessive inheritance. In patient 3, who has consanguineous parents, we identified homozygous regions (appendix), in which we searched for homozygous mutations. One paediatric patient came from a family with X-linked disease inheritance, and

this family participated in another exome sequencing study focused on X-linked disorders. We then used Sanger sequencing to sequence the *CLCN2* gene in both the adult and paediatric patients; *GJB1,* which encodes the gap junction beta-1 protein (also known as connexin 32), was sequenced in the male patient without *CLCN2* mutations (appendix).

CLCN2 mRNA was quantified in fibroblasts of adult patients with *CLCN2* mutations. Transient transfections of wild-type or mutant ClC-2-V5-His6 expression plasmids in COS7 cells were used to study the functional effects of *CLCN2* mutations (appendix).

To define which cell types express ClC-2 in healthy mature human brain, we examined the posterior limb of the internal capsule, frontal white matter, frontal cortex, and ependyma with fluorescence immunohistochemistry of tissue obtained at autopsy from nine patients aged 1–75 years (appendix) who succumbed to heart disease or extracerebral neoplasm. None of the patients had neurological symptoms and neuropathological examination showed no abnormalities.

Immunohistochemistry (appendix) was done on frozen tissue using antibodies against ClC-2, GlialCAM, MLC1, glial fibrillary acidic protein (GFAP; an astrocyte marker), oligodendrocyte transcription factor-2 (OLIG2; an oligodendrocyte marker), neuronal nuclear antigen (NeuN; a neuronal marker, also known as RBFOX3), platelet endothelial cell adhesion molecule-1 (PECAM1; an endothelial marker, also known as CD31), and phosphorylated and non-phosphorylated neurofilament H (SMI31 and SMI32, respectively; axonal markers). The anti-ClC-2 antibodies were validated for specificity (appendix). All sections were counterstained with DAPI (4',6-diamidino-2-phenylindole; nuclear staining).

Electron microscopy was done on tissue from the posterior limb of the internal capsule (appendix). Sections were incubated with ClC-2, GlialCAM, and MLC1 antibodies.

Role of the funding source

The sponsors of the study had no role in study design, data collection, data analysis, data interpretation, or writing of the report. The corresponding authors had full access to all the data in the study and had final responsibility for the decision to submit for publication.

Results

Seven patients met our inclusion criteria, three with adult-onset disease and four with childhood-onset disease. The three patients with adult-onset disease were unrelated (patients 1–3; table 1). They had mild cerebellar ataxia and a variable combination of chorioretinopathy with visual field defects, optic neuropathy, and headaches. One patient had a schizophrenia-like disorder. The three patients with childhood-onset disease and *CLCN2* mutations (patients 4–6) had mild cerebellar ataxia and a variable combination of mild spasticity, visual field defects, learning disabilities, and headaches (table 1).

The patient with X-linked disease (patient 7; table 1) presented with nystagmus at 12 months. He developed incapacitating cerebellar ataxia and spasticity. Clinical evidence of peripheral nerve involvement was absent, although recent neurophysiological investigations revealed mild motor neuropathy. Affected male family members had the same clinical and MRI findings. Carrier females had no abnormalities.

All patients had prominent signal abnormalities and decreased ADC values in the posterior limbs of the internal capsules, cerebral peduncles in the midbrain, pyramidal tracts in the pons, and middle cerebellar peduncles (fig. 1; appendix). All patients with adult-onset disease had additional signal abnormalities in specific brainstem tracts and the cerebellar white matter (appendix). Cerebral hemispheric white matter abnormalities were mild and non-specific. In one patient (patient 1), low to borderline-low ADC values were also found in cerebral white matter areas (appendix).

In the paediatric patients, the same additional signal abnormalities in specific brainstem tracts and cerebellum were noted. Additionally, they had diffuse mild signal abnormality of the brain white matter, which was hyperintense relative to grey matter on T2-weighted and T1-weighted images (fig. 1). Low to borderline-low ADC values were present in the cerebral and cerebellar hemispheric white matter and corpus callosum. The signal behaviour of the white matter on T1-weighted and T2-weighted images would typically suggest hypomyelination (Schiffmann & van der Knaap, 2009), but hypomyelination is associated with increased size of water spaces and therefore increased ADC values (Dreha-Kulaczewski et al., 2012). The low white matter ADC suggests myelin microvacuolation instead of hypo myelination (Patay, 2005). Increased intramyelinic water accounts for the mild T2-signal changes.

As a result of exome sequencing and homozygosity mapping in patient 3, we identified ten homozygous single nucleotide substitutions and two homozygous insertion-deletions with a possible effect on gene or protein function that were absent from control databases (appendix). One was a homozygous in-frame deletion (p.Leu144_Ile145del) in *CLCN2*. Analysis of exome data in the other adult patients revealed the same homozygous non-sense mutation (p.Trp570X) in *CLCN2* (table 2; appendix). *CLCN2* was the only gene that contained at least one homozygous or at least two heterozygous, possibly deleterious variants in all three patients that were absent from exome data from individuals with other diseases analysed at the same time (appendix).

Analysis of the coding sequence of *CLCN2* by Sanger sequencing in the paediatric patients identified homozygous or compound-heterozygous *CLCN2* mutations in three patients (table 2; appendix). All mutations were predicted to be pathogenic and none was present in healthy controls of the same origin or in the International Hapmap Project and the 1000 Genomes Project databases (appendix).

Sequencing of the exome of the paediatric patient without *CLCN2* mutations who had an X-linked family history revealed a novel missense mutation (p.Pro174Ser) in *GJB1* (table 2; appendix). This mutation was confirmed in his mother and in one living similarly affected male family member.

Quantification of the *CLCN2* mRNA in fibroblasts from patients and controls by real-time quantitative PCR showed that the mRNA with the p.Trp570X mutation was substantially downregulated compared with that of controls, by contrast with the mRNA with p.Leu144_Ile145del (appendix). Treatment with emetine, an inhibitor of non-sense mediated decay, rescued the mRNA expression, suggesting that p.Trp570X leads to degradation of the mutant mRNA, although a substantial fraction of the mRNA subsists. We could not confirm the presence of the truncated protein because expression of ClC-2 was undetectable in fibroblasts. Transient expression of the protein with the p.Trp570X mutation in COS7 cells showed that the truncated protein, if expressed, has an aberrant localisation restricted to the Golgi apparatus (appendix).

The p.Leu144_Ile145del and p.Ala500Val mutations are thought to affect conserved hydrophobic aminoacids located in transmembrane domains of ClC-2, possibly leading to protein misfolding or misinsertion in the membrane. To test this hypothesis, we compared the expression and subcellular localisation of V5-His6-tagged ClC-2 with the p.Leu144_Ile145del or p.Ala500Val mutation to those of the wild-type protein in COS7 cells. Localisation of the p.Leu144_Ile145del

Table 1. Clinical findings

	Patient 1	Patient 2	Patient 3	Patient 4	Patient 5	Patient 6	Patient 7
Year of birth	1948	1952	1961	1996	1998	2001	1993
Sex / ancestry	f / North Africa	f / North Africa	f / North Africa	f / Europe	m / Europe	f / Europe	m / Europe
Consanguineous parents	no	no	yes	not known	no	yes	no
Affected family members	no	no	no	no	no	no	yes
Early psychomotor development	normal	normal	normal	normal	normal	normal	normal, but has never walked without support
Age at first sign	44 years	57 years	30 years	12 years	6 years	3 years	12 months
Presenting signs	action tremor, mild gait ataxia	tinnitus, vertigo	chorioretinopathy, psychosis	learning disability, headache	headache	action tremor, mild gait ataxia	nystagmus
Disease course	stable	progressive	stable	stable	stable	stable	slowly progressive
Signs of the deterioration	none	deafness	none	none	none	none	motor deterioration
Headache	no	no	yes	yes, severe	yes, severe	no	no
Cognitive level	normal	normal	severe learning disability	mild learning disability	normal	mild learning disability	mild learning disability
Head circumference	normal	normal	normal	normal	normal	borderline macrocephaly	borderline macrocephaly
Vision	normal	20/80 right eye; 20/400 left eye	1/10 right eye; 1/50 left eye	normal with glasses	normal with glasses, strabismus	normal	normal
Visual field defects	no	yes	yes	yes	no	yes	no

Table 1 (cont.). Clinical findings

	Patient 1	Patient 2	Patient 3	Patient 4	Patient 5	Patient 6	Patient 7
Retina and optic nerve	normal	retinoschisis, bilat optic neuropathy	retinal atrophy, choroidal neovascularisation, bilat optic neuropathy	normal	normal	normal	normal
Nystagmus	no	no	no	no	yes	no	yes
Hearing	normal	perceptive hearing loss	normal	normal	normal	normal	normal
Spasticity	no	no	no	yes, mild	no	yes, mild	yes, prominent
Ataxia	yes, mild	yes, mild	yes, mild	yes, mild	yes, mild	yes, mild	yes, severe
Peripheral polyneuropathy	no	no	no	no	no	no	no clinical signs; mildly decreased motor NCV
Gait	unstable	unstable	unstable	unstable	normal	unstable	wheelchair dependent

f: female. m: male. NCV: nerve conduction velocity.

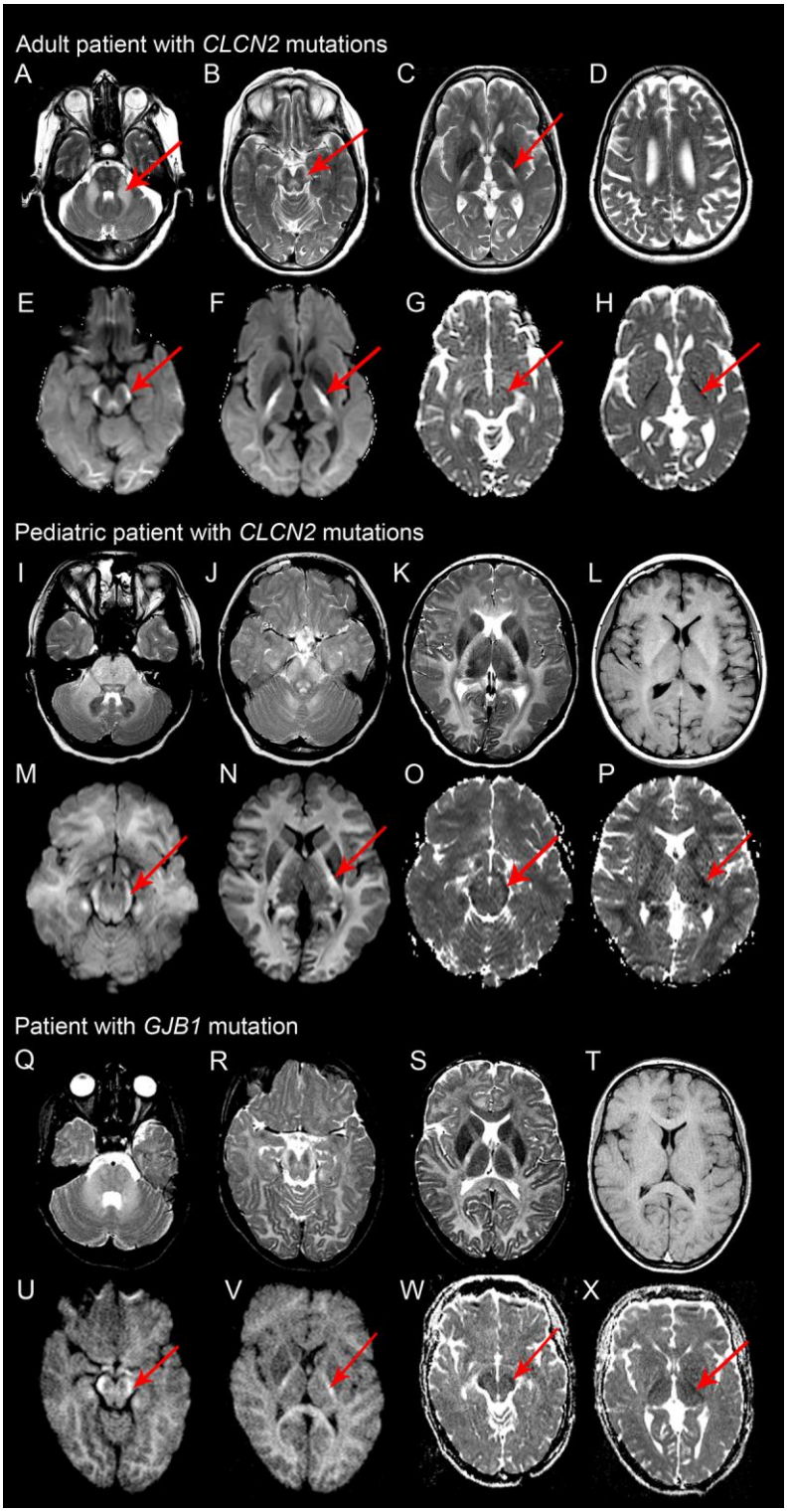
Adult patient with *CLCN2* mutations
A
B
C
D
E
F
G
H
Pediatric patient with *CLCN2* mutations
I
J
K
L
M
N
O
P
Patient with *GJB1* mutation
Q
R
S
T
U
V
W
X

ClC-2 and p.Ala500Val ClC-2 proteins was restricted to the endoplasmic reticulum, whereas wild-type ClC-2 was present in different subcellular compartments including the plasma membrane (fig. 2A). Additionally, the amount of both mutated ClC-2 proteins transiently expressed in COS7 cells was lower than the amount of wild-type ClC-2 (fig. 2B) and the mutated proteins hardly reached the plasma membrane (fig. 2C,D). These findings suggest that p.Leu144_Ile145del ClC-2 and p.Ala500Val ClC-2 are trapped and degraded in the endoplasmic reticulum. Altogether, these results suggest that all mutations identified in the patients led to a complete or at least partial loss of function of the ClC-2 channel by different mechanisms.

Immunohistochemistry of the healthy brain samples revealed that virtually all GFAP-positive fibrous astrocytes in the posterior limb of the internal capsule and frontal white matter express ClC-2 on the surface of cell bodies and processes (fig. 3A). ClC-2 immunopositivity had a fine punctate quality (fig. 3A, inset), as expected for a membrane protein. Many ClC-2-positive astrocytic processes ran parallel and perpendicular to axonal bundles (fig. 3A) and abutting axons (appendix). ClC-2 was enriched in perivascular astrocytes (fig. 3B), where GlialCAM (Fig. 3C; appendix) and MLC1 (appendix) were also expressed. GlialCAM and MLC1

Figure 1. MRI of brain in patients 1, 4, and 7. MRI in patient 1 at the age of 63 years (**A–H**) shows signal abnormalities on T2-weighted images (A–D) in the middle cerebellar peduncles (arrow in A), midbrain cerebral peduncles (arrow in B), and posterior limbs of the internal capsules (arrow in C). Slight signal abnormalities are present in the cerebral white matter (D). Diffusion-weighted images (E, F) show high signal in the midbrain cerebral peduncles (arrow in E), posterior limbs of the internal capsules (arrow in F), and to a lesser extent the posterior subcortical cerebral white matter (compare hyperintense posterior white matter to normal anterior white matter in E and F), suggesting restricted diffusion, confirmed by low ADC values on the ADC maps (low signal in G and H, arrows). MRI in patient 4 at the age of 14 years (**I–P**) shows diffuse mild T2-hyperintensity (I–K) and T1-hyperintensity (L) of all white matter structures. Prominent T2-hyperintensity is seen in the basis pontis (I), middle cerebellar peduncles (I), midbrain cerebral peduncles (J), and posterior limbs of the internal capsules (K). Diffusion-weighted images (M, N) show increased signal in virtually all white matter, especially the midbrain cerebral peduncles (arrow in M) and posterior limbs of the internal capsules (arrow in N), suggesting restricted diffusion, confirmed by low ADC values on the ADC maps (arrows in O and P). MRI in patient 7 at the age of 14 years (**Q–X**) shows diffuse mild T2-hyperintensity (Q–S) and T1-hyperintensity (T) of all white matter structures. Prominent T2-hyperintensity is seen in the middle cerebellar peduncles (Q), midbrain cerebral peduncles (R), and posterior limbs of the internal capsules (S). Diffusion-weighted images (U, V) show mildly increased signal in almost all white matter, especially the midbrain cerebral peduncles (arrow in U) and posterior limbs of the internal capsules (arrow in V), suggesting restricted diffusion, confirmed by low ADC values on the ADC maps (arrows in W and X).

Table 2. *CLCN2* and *GJB1* mutations

	Exon	DNA	RNA	Protein	Genotype	Confirmation in parents*
CLCN2 mutation						
Patient 1	15	c.1709G→A	--	p.Trp570X	homozygous	--
Patient 2	15	c.1709G→A	--	p.Trp570X	homozygous	--
Patient 3	4	c.430_435del	--	p.Leu144_Ile145del	homozygous	--
Patient 4	11; 2 to part of 6	c.1143delT; c.64–1107_639del	r.1143delt; r.64_639delins82†	p.Gly382AlafsX34; p.Met22LeufsX5	heterozygous; heterozygous	--
Patient 5	14	c.1499C→T	r.1499c→t	p.Ala500Val	homozygous	father and mother
Patient 6	8	c.828dupG	--	p.Arg277AlafsX23	homozygous	father and mother
GJB1 mutation						
Patient 7	2	c.520C→T	--	p.Pro174Ser	hemizygous	mother

*This column shows whether the mutation was confirmed in the father and mother of the affected patient. †Comprises a deletion of exons 2–5 and part of exon 6 and the insertion of intron 1 c.63+1097_64−1108.

immunoreactivity overlapped consistently and extended further distally than ClC-2 into astrocytic endfeet approaching the basal lamina (fig. 3C; appendix). A more discrete, punctate ClC-2 immunoreactivity was visible intermittently along axons (appendix). We detected many ClC-2-positive and GFAP-negative cells with the morphology of oligodendrocytes. In the frontal cortex, ClC-2 expression was detected only in scattered protoplasmic astrocytes around blood vessels and in astrocytes that are part of the glia limitans (fig. 3D; appendix). In these locations, ClC-2 astrocytes coexpressed GlialCAM (fig. 3E; appendix) and MLC1 (appendix). ClC-2 expression was also detected in the ependymal lining, again overlapping with GlialCAM (fig. 3F; appendix) and MLC1 (appendix). No ClC-2-positive expression was noted in neuronal perikarya (fig. 3G).

Electron microscopy confirmed that ClC-2 was abundantly present in white matter astrocytes and enriched in cell processes contacting abaxonal myelin (fig. 4A) and contacting each other (fig. 4B). At these sites, GlialCAM showed a similar distribution (fig. 4C,D). ClC-2 immunoreactivity was also visible inside axons and at the axonal surface contacting adaxonal myelin (appendix). By contrast, GlialCAM and MLC1 were not detected in axons or myelin (fig. 4C). Around blood vessels, ClC-2 was found at astrocyte–astrocyte contacts in endfeet (fig. 4B), a site where GlialCAM (fig. 4D) and MLC1 (fig. 4E) were present.

Discussion

We showed that autosomal recessive loss-of-function mutations in *CLCN2* cause a leukoencephalopathy with MRI evidence of myelin microvacuolation. These findings are similar to those in ClC-2-deficient mice and are in line with the notion that ClC-2 in the brain is involved in ion and water homoeostasis (panel) (Bosl et al., 2001; Blanz et al., 2007).

Our observations do not support the hypothesis that loss-of-function mutations in *CLCN2* confer an increased risk of epilepsy. None of the six patients with homozygous or compound heterozygous mutations in *CLCN2* had epilepsy or a family history of epilepsy, suggesting that partial or complete ClC-2 loss of function per se is insufficient to cause epilepsy.

The disease associated with *CLCN2* mutations is variable in age of onset and clinical presentation. Mild cerebellar ataxia is the most consistent finding. Retinopathy, as reported in the ClC-2-deficient mice, was detected in only some of the patients, although the visual field defects in absence of other ophthalmological

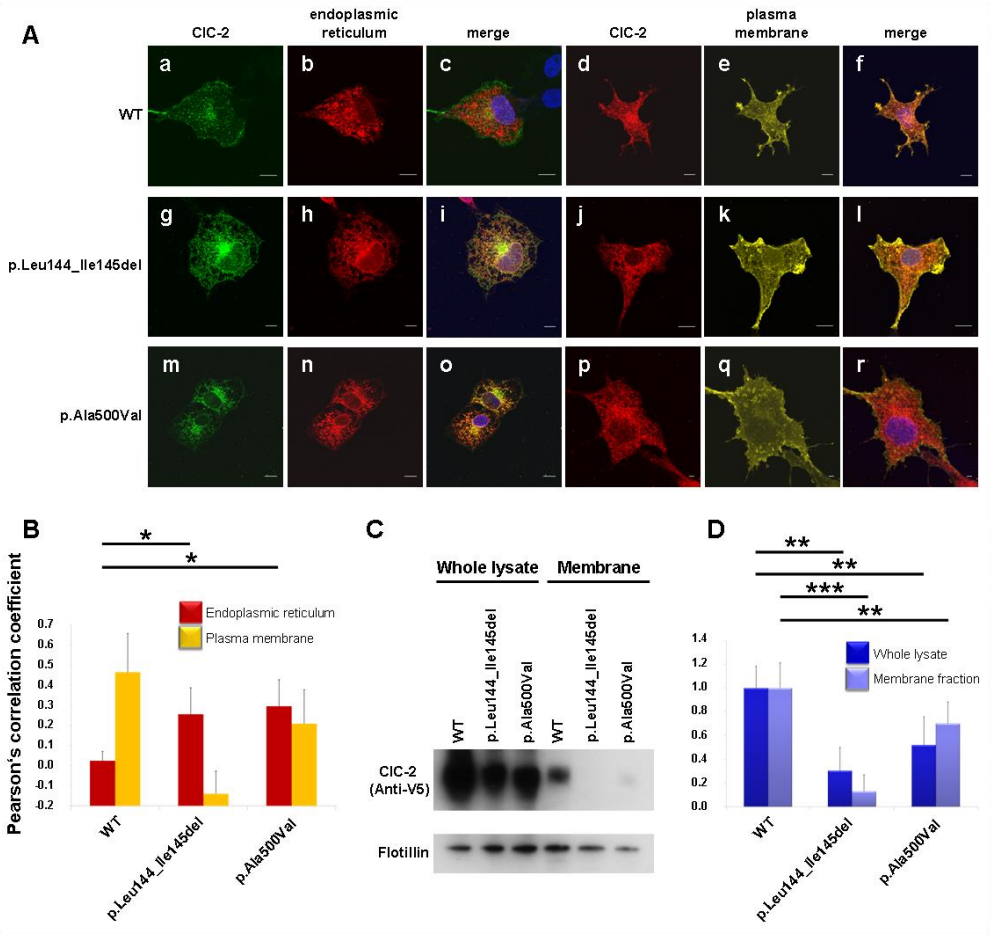

Figure 2. Functional effects of *CLCN2* mutations. (**A**) Subcellular localisation of wild-type (a-f) and mutated (p.Leu144_Ile145del [g-l]; p.Ala500Val [m-r) ClC-2 proteins and colocalisation with markers of endoplasmic reticulum (anti-calreticulin, red) or plasma membrane (pEYFP-Mem, yellow) by confocal microscopy. Note that wild-type ClC-2 is present at the plasma membrane and different subcellular compartments, whereas both mutant proteins are mainly seen in the endoplasmic reticulum. Scale bar=10 µm. (**B**) Quantification of colocalisation of wild-type or mutated ClC-2 with endoplasmic reticulum and plasma membrane using Pearson's correlation coefficient, including at least three cells per group. (**C**) Analysis of wild-type and mutated ClC-2 protein expression in whole lysates and plasma membranes by Western blot show that the amount of mutant ClC-2 protein transiently expressed in COS7 cells is decreased compared to the wild-type form, especially in the plasma membrane. The image shows the result of a representative experiment. Flotillin was used to control and normalise the protein load. (**D**) Quantification of wild-type and mutant ClC-2 proteins present in whole lysates and in plasma membranes shows that, overall, mutant ClC-2 proteins are not as frequently expressed as wild-type ClC-2, suggesting that they are misfolded and instable. By contrast with the wild- type form, both mutants are retained in the endoplasmic reticulum where they are probably degraded and hardly reach the plasma membrane. The values, obtained from at least three different experiments, were compared with the Mann-Whitney test. *p<0.05. **p<0.01. ***p<0.001.

findings suggest that the other patients might have had a retinopathy that was too subtle to be picked up at funduscopy. ClC-2-deficient mice are sterile because of testicular degeneration; however, the only male patient with *CLCN2* mutations (aged 15 years) did not yet show signs of testicular degeneration. Although the clinical presentation of the patients is non-specific and does not allow a diagnosis, MRI findings in these patients are highly specific and do allow a diagnosis. We have also analysed the *CLCN2* gene in several other adult and paediatric patients who had similar MRI findings to those of study patients, but did not meet the MRI inclusion criteria, and we did not find *CLCN2* mutations in any of them (data not shown).

The phenotypic variability reported in the patients might at least in part be related to the extent of ClC-2 loss of function. Both the mutational variation and functional analyses suggest loss of function of ClC-2, but some mutated proteins, in particular C-terminally truncated or missense mutants that reach the plasma membrane in substantial amounts, could possibly retain a partial function.

The present study adds to the growing insight into how the brain deals with the continuous shifts of ions and water related to action potentials. Brain white matter mainly consists of myelinated axons and its most important physiological function is impulse conduction. Action potentials are based on shifts in ions, which are obligatorily associated with osmotically driven shifts in water, needing rapid compensation. Any disturbance of the compensatory mechanisms might disrupt impulse transmission or lead to life-threatening changes in brain volume. Brain ion and water homoeostasis is complex and involves electrolytes and organic osmolytes, channels, and transporters, and coordinated processes such as regulatory volume decrease and increase to correct cell volume changes (Benfenati & Ferroni, 2010; Rash, 2010). Astrocytes are central in this process. They are the most abundant and best connected cell type of the so-called panglial syncytium, a vast network of astrocytes, oligodendrocytes, and ependymal cells interconnected by gap junctions. The panglial syncytium is essential for long-distance disposal of ions and water (Benfenati & Ferroni, 2010; Rash, 2010).

Action potentials are associated with disposal of submyelinic and intramyelinic potassium (Rash, 2010). In myelinated axons, depolarisation is associated with influx of sodium at nodes of Ranvier; compensatory potassium efflux occurs in paranodal regions covered by myelin (appendix).
Gap junctions help to transport potassium and osmotic water across myelin layers into astrocytes. Connexin 32 constitutes gap junctions in paranodal myelin;

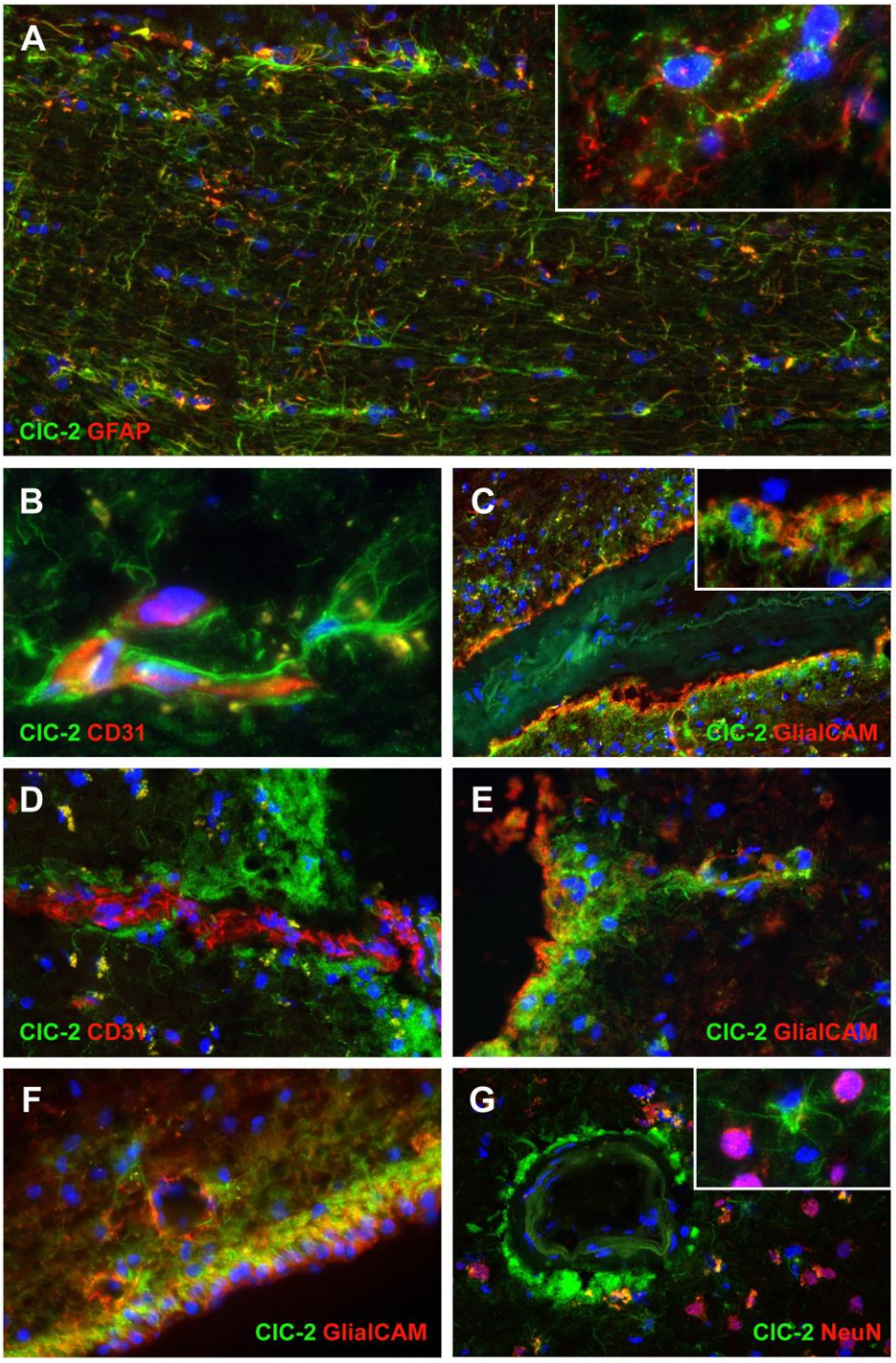
A
ClC-2 GFAP
B
ClC-2 CD31
C
ClC-2 GlialCAM
D
ClC-2 CD31
E
ClC-2 GlialCAM
F
ClC-2 GlialCAM
G
ClC-2 NeuN

connexin 32 and connexin 47 constitute gap junctions between myelin and astrocytes. The astrocytic syncytium allows rapid dispersion of potassium and buffers the associated volume changes. This process of so-called potassium siphoning prevents action-potential-induced osmotic intramyelinic oedema (Rash, 2010). Disruptions of molecular components of these ion and water homoeostatic pathways are associated with intramyelinic oedema in human diseases and mutant mouse models (Blanz et al., 2007; Edwards et al., 2010; Rash, 2010; Neusch et al., 2001; Menichella et al., 2006). No myelin vacuolation occurs in mouse models in the absence of action potentials (Blanz et al., 2007; Neusch et al., 2001), showing that hindrance of compensation of action-potential-induced ion and water shifts is the main factor leading to osmotic intramyelinic oedema.

Insight into the mechanisms and molecular components of brain ion and water homoeostatic pathways is still incomplete. Our study provides evidence that ClC-2 is one of these molecular components. The first observation that supports a role of ClC-2 in brain ion and water homoeostasis is the MRI evidence of myelin microvacuolation in patients with *CLCN2* mutations. The second observation is the presence of the same MRI abnormalities with evidence of myelin microvacuolation in a patient with a *GJB1* mutation. Mutations in *GJB1,* encoding connexin 32, lead to X-linked Charcot-Marie-Tooth disease. In addition to peripheral neuropathy, patients with X-linked Charcot-Marie-Tooth disease might have episodes of brain dysfunction, with MRI evidence of transient myelin vacuolation (Paulson et al.,

Figure 3*:* Immunohistochemistry: expression of ClC-2 in a healthy adult human brain. Double staining of the cerebral white matter for ClC-2 (green) and the astrocyte-specific marker GFAP (red) shows that all GFAP-positive astrocytes express ClC-2 (A). Note the long ClC-2-positive astrocytic processes extending parallel and perpendicular to the direction of the fibre bundle. ClC-2 shows a punctuate immunoreactivity, as expected for a membrane protein (inset in A). Colabelling of the same tissue for ClC-2 (green) and the vascular endothelial cell marker CD31 (also known as PECAM1; red) shows that expression of ClC-2 is enhanced in the astrocytes surrounding the blood vessels deep in the parenchyma (B) and the penetrating vessels at the surface of the brain (D). Note the many fine astrocytic processes running along the white matter capillary (B). Perivascular astrocytes (C), subpial astrocytes (E), and ependymal cells (F) coexpress GlialCAM (red) with ClC-2 (green), but GlialCAM immunoreactivity extends further into the astrocytic processes and endfeet (inset in C). Double staining of the frontal cortex for ClC-2 (green) and the neuronal marker NeuN (red) shows that, in this location, ClC-2 immunoreactivity is restricted to perivascular astrocytes (G). No ClC-2 expression is seen in the NeuN-positive neuronal cells (inset in G). In all images the cell nuclei are stained with DAPI (4´,6-diamidino-2-phenylindole; blue). Original magnifications: (A) 100×, (B) 630×, (C– G) 200×, (insets) 400×.

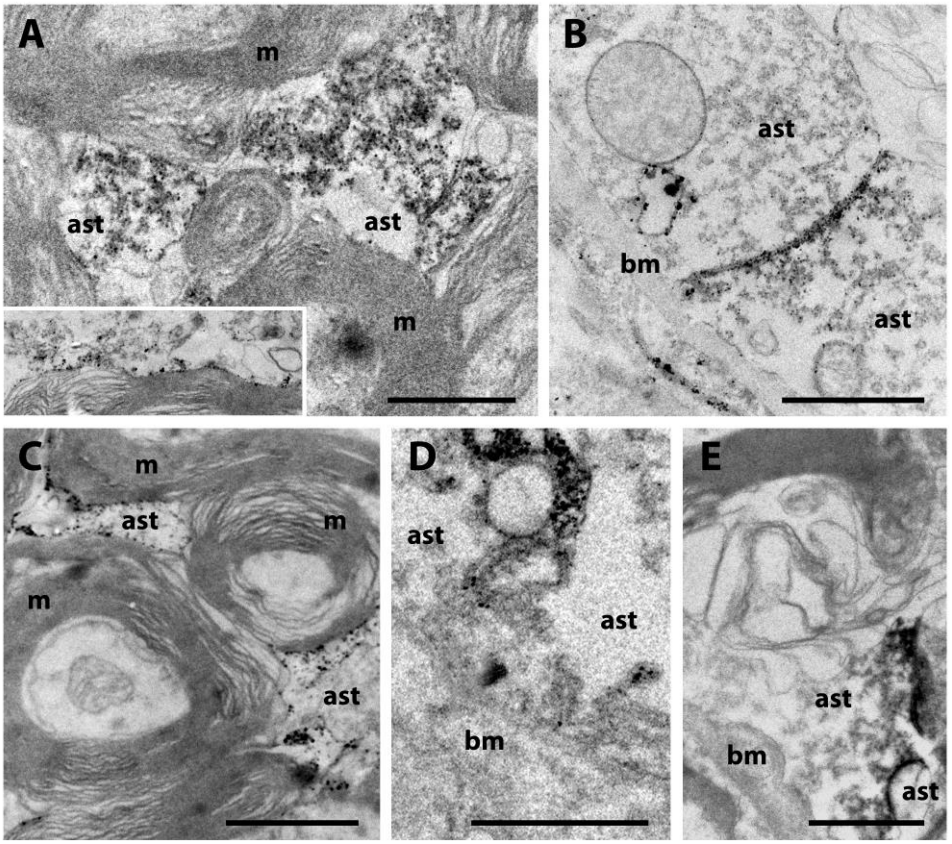

Figure 4*:* Electron microscopy: ClC-2, GlialCAM, and MLC1 immunoreactivity in the healthy adult white matter. ClC-2 is expressed on astrocytic processes in between myelinated axons (**A**) and in contact with abaxonal myelin (inset in A). A similar localisation is observed for GlialCAM (**C**). Intense ClC-2 immunoreactivity is present in astrocytic endfeet surrounding blood vessels (**B**). Note the enhanced ClC-2 expression in the astrocyte–astrocyte contacts of the endfeet (B). At this site, GlialCAM (**D**) and MLC1 (**E**) are also expressed. Scale bars=1 μm. ast=astrocyte. bm=basement membrane. m=myelin.

2002). We have no explanation for why the mutation detected in the family that we studied has a persistent effect on brain myelin, without any fluctuation, both clinically and on serial MRI. The serious spasticity and cerebellar ataxia probably over shadow the neuropathy, which was only detected by neurophysiological studies after the *GJB1* mutation had been identified. Other cases of X-linked Charcot-Marie-Tooth disease with persistent clinical signs of brain dysfunction and

white matter disease on MRI have been reported, but diffusion findings were not mentioned (Siskind et al., 2009). The third observation supporting the role of ClC-2 in brain ion and water homoeostasis is the ClC-2 membrane expression in the panglial syncytium, with enhanced expression around blood vessels, in the glia limitans, ependymal lining, and astrocyte–astrocyte contacts in the white matter. The fourth observation is the finding that ClC-2 colocalises with MLC1 and GlialCAM in astrocytic endfeet at the perivascular basal lamina and glia limitans (Lopez-Hernandez et al., 2011; Jeworutzki et al., 2012; Boor et al., 2005). As recently reviewed (van der Knaap et al., 2012), both *GLIALCAM* and *MLC1* mutations cause megalencephalic leukoencephalopathy with subcortical cysts (Leegwater et al., 2001; Lopez-Hernandez et al., 2011), a disease characterised by myelin vacuolation in the cerebral white matter, in which the corpus callosum, internal capsule, brainstem, and cerebellum are spared in comparison (van der Knaap et al., 1995 & 1996). MLC1 is involved in chloride currents necessary for the astrocytic regulatory volume decrease after cell swelling (Ridder et al., 2011). GlialCAM is indispensable for correct localisation of MLC1 and ClC-2 (Lopez-Hernandez et al., 2011; Jeworutzki et al., 2012). Results of our study suggest that ClC-2 is part of the same ion and water homoeostatic pathways as MLC1 and GlialCAM (appendix).

A limitation of our study is the rather small number of patients. The database on unclassified leukoencephalopathies in Amsterdam contains more than 3000 patients, but only a few patients fulfilled the MRI criteria. It could be that the ClC-2-related leukoencephalopathy is very rare, but we cannot exclude the possibility that the phenotypic variation is much wider and that we have not analysed a sufficient number of patients yet. Another issue is the specificity of the antibody against human ClC-2. To provide full proof, absence of all staining should be shown in brain tissue of a patient with two *CLCN2* null mutations. This tissue is not available. However, we did several experiments that support the specificity of the antibody and thus the validity of the immunohistochemical data (appendix).

Many questions remain. The exact role of ClC-2 in brain ion and water homoeostasis is unknown. Why defects in the same pathways cause different white matter disorders is unclear. ClC-2-related and connexin-32-related diseases preferentially affect white matter structures that are spared (relatively) by MLC1-related and GlialCAM-related disease. Although recessive mutations in *MLC1* and *GLIALCAM* lead to diff use cerebral white matter oedema, sparing the corpus callosum, internal capsule, brainstem, and cerebellum, recessive mutations in *CLCN2* and *GJB1* preferentially cause white matter oedema of the internal

capsule, brainstem structures, and cerebellum. Another intriguing question concerns the size of the myelin vacuoles. In MLC, ADC values in the affected white matter are highly increased (van der Voorn et al., 2006), suggesting large vacuoles and increased extracellular spaces, as confirmed by electron microscopy (van der Knaap et al., 1996). In ClC-2-related and connexin-32-related disease, ADC values in affected white matter are low, suggesting small intramyelinic vacuoles and extracellular spaces. Although GlialCAM is supposed to be a chaperone for both MLC1 and ClC-2 (Lopez-Hernandez et al., 2011; Jeworutzki et al., 2012), recessive *GLIALCAM* mutations lead to a disease that is indistinguishable from the disease caused by *MLC1* mutations and does not share the MRI features of the disease caused by *CLCN2* mutations (Lopez-Hernandez et al., 2011). We noted that GlialCAM and MLC1 share restricted localisation in distal astrocytic processes, whereas ClC-2 has a more diffuse membrane localisation in astrocytes. These disease observations suggest that GlialCAM is a straightforward chaperone for MLC1, but that its relation with ClC-2 is more complex.

The growing group of known disorders affecting brain ion and water homoeostasis are typically relatively mild compared with other brain disorders, both in mice (Bosl et al., 2001; Blanz et al., 2007; Edwards et al., 2010; Menichella et al., 2006) and human beings (van der Knaap et al., 1995 & 2010; Lopez-Hernandez et al., 2011; Paulson et al., 2002). The importance of the volume regulation process in the brain is emphasised by the observation that it does not rely on just one protein or one pathway. Mutations in one protein only lead to partial and sometimes transient dysfunction. It is important to note that intramyelinic oedema can be reversible. Patients with megalencephalic leukoencephalopathy with subcortical cysts, caused by dominant *GLIALCAM* mutations, improve or recover spontaneously (van der Knaap et al., 2010; Lopez-Hernandez et al., 2011). In most patients with a *GJB1* mutation, the white matter disease is transient (Paulson et al., 2002). If means are found to target components of the ion and water homoeostatic pathways, myelin oedema might be successfully combated.

Acknowledgments

We thank patients and families for their participation in the study. We thank the following practitioners for their identification and referral of patients: Janell Kierstein, Johan van Hove, and Abigail Collins from the Children's Hospital of Denver, and Johanna L Schmidt, Children's National Medical Center, Washington. We thank Raúl Estévez, University of Barcelona, for the anti-MLC1 antibody, and

the Dutch Brain Bank for providing part of the tissue used in the study. We thank James M Powers, University of Rochester, for critical reading of the manuscript. We thank the PIC-PS platform of Centre de Recherche de l'Institut du Cerveau et de la Moelle Epinière (CRICM) and the genotyping and sequencing platform of L'Institut du Cerveau et de la Moelle Épinière for technical assistance; the DNA and cell bank of CRICM for DNA extraction and cell culture; Kees van Rozendaal, Department of Clinical Genomics, Maastricht University Medical Center, for assistance in the exome sequencing of patient 7 and his family; and Petra J W Pouwels, VU University Medical Center, Amsterdam, for her help with the analysis of the apparent diffusion coefficient maps.

Funding was provided by European Leukodystrophies Association, INSERM and Assistance Publique–Hôpitaux de Paris, Dutch Organisation for Scientific Research (ZonMw), E-Rare, Hersenstichting, Optimix Foundation for Scientific Research, Myelin Disorders Bioregistry Project, National Institute of Neurological Disorders and Stroke, and Genetic and Epigenetic Networks in Cognitive Dysfunction (GENCODYS) Project (funded by the European Union Framework Programme 7).

References

Benfenati V & Ferroni S. Water transport between CNS compartments: functional and molecular interactions between aquaporins and ion channels. Neuroscience 2010;168:926-940.

Blanz J et al. Leukoencephalopathy upon disruption of the chloride channel ClC-2. J Neurosci 2007;27:6581-6589.

Boor PK et al. MLC1: a novel protein in distal astroglial processes. J Neuropathol Exp Neurol 2005;64:412-419.

Bosl MR et al. Male germ cells and photoreceptors, both dependent on close cell-cell interactions, degenerate upon ClC-2 Cl(-) channel disruption. EMBO J 2001;20:1289-1299.

Combi R et al. Clinical and genetic familial study of a large cohort of Italian children with idiopathic epilepsy. Brain Res Bull 2009;79:89-96.

D'Agostino D et al. Mutations and polymorphisms of the CLCN2 gene in idiopathic epilepsy. Neurology 2004;63:1500-1502.

Dreha-Kulaczewski SF et al. Assessment of myelination in hypomyelinating disorders by quantitative MRI. J Magn Reson Imaging 2012;36:1329-1338.

Edwards MM et al. Photoreceptor degeneration, azoospermia, leukoencephalopathy, and abnormal RPE cell function in mice expressing an early stop mutation in CLCN2. Invest Ophthalmol Vis Sci 2010;51:3264-3272.

Everett K et al. Linkage and mutational analysis of CLCN2 in childhood absence epilepsy. Epilepsy Res 2007;75:145-153.

Grunder S et al. Regions involved in the opening of CIC-2 chloride channel by voltage and cell volume. Nature 1992;360:759-762.

Haug K et al. Retraction: Mutations in CLCN2 encoding a voltage-gated chloride channel are associated with idiopathic generalized epilepsies. Nat Genet 2009;41:1043.

Jeworutzki E et al. GlialCAM, a protein defective in a leukodystrophy, serves as a ClC-2 Cl(-) channel auxiliary subunit. Neuron 2012;73:951-961.

Jordt SE & Jentsch TJ. Molecular dissection of gating in the ClC-2 chloride channel. EMBO J 1997;16:1582-1592.

Kleefuss-Lie A et al. CLCN2 variants in idiopathic generalized epilepsy. Nat Genet 2009;41:954-955.

Leegwater PA et al. Mutations of MLC1 (KIAA0027), encoding a putative membrane protein, cause megalencephalic leukoencephalopathy with subcortical cysts. Am J Hum Genet 2001;68:831-838.

Lopez-Hernandez T et al. Mutant GlialCAM causes megalencephalic leukoencephalopathy with subcortical cysts, benign familial macrocephaly, and macrocephaly with retardation and autism. Am J Hum Genet 2011;88:422-432.

Menichella DM et al. Genetic and physiological evidence that oligodendrocyte gap junctions contribute to spatial buff ering of potassium released during neuronal activity. J Neurosci 2006;26:10984-10991.

Neusch C et al. Kir4.1 potassium channel subunit is crucial for oligodendrocyte development and in vivo myelination. J Neurosci 2001;21:5429-5438.

Niemeyer MI et al. No evidence for a role of CLCN2 variants in idiopathic generalized epilepsy. Nat Genet 2010;42:3.

Patay Z. Diffusion-weighted MR imaging in leukodystrophies. Eur Radiol 2005;15:2284-2303.

Paulson HL et al. Transient central nervous system white matter abnormality in X-linked Charcot-Marie-Tooth disease. Ann Neurol 2002;52:429-434.

Planells-Cases R & Jentsch TJ. Chloride channelopathies. Biochim Biophys Acta 2009;1792:173-189.

Rash JE. Molecular disruptions of the panglial syncytium block potassium siphoning and axonal saltatory conduction: pertinence to neuromyelitis optica and other demyelinating diseases of the central nervous system. Neuroscience 2010;168:982-1008.

Ratte S & Prescott SA. ClC-2 channels regulate neuronal excitability, not intracellular chloride levels. J Neurosci 2011;31:15838-15843.

Ridder MC et al. Megalencephalic leucoencephalopathy with cysts: defect in chloride currents and cell volume regulation. Brain 2011;134:3342-3354.

Rinke I et al. ClC-2 voltage-gated channels constitute part of the background conductance and assist chloride extrusion. J Neurosci 2010;30:4776-4786.

Schiffmann R & van der Knaap MS. Invited article: an MRI-based approach to the diagnosis of white matter disorders. Neurology 2009;72:750-759.

Saint-Martin C et al. Two novel CLCN2 mutations accelerating chloride channel deactivation are associated with idiopathic generalized epilepsy. Hum Mutat 2009;30:397-405.

Scheper GC et al. Analysis of CLCN2 as candidate gene for megalencephalic leukoencephalopathy with subcortical cysts. Genet Test Mol Biomarkers 2010;14:255-257.

Sik A et al. Distribution of chloride channel-2-immunoreactive neuronal and astrocytic processes in the hippocampus. Neuroscience 2000;101:51-65.

Siskind C et al. Persistent CNS dysfunction in a boy with CMT1X. J Neurol Sci 2009;279:109-113.

Smith RL et al. Differential expression of an inwardly rectifying chloride conductance in rat brain neurons: a potential mechanism for cell-specific modulation of postsynaptic inhibition. J Neurosci 1995;15:4057-4067.

Stogmann E et al. Mutations in the CLCN2 gene are a rare cause of idiopathic generalized epilepsy syndromes. Neurogenetics 2006;7:265-268.

Thiemann A et al. A chloride channel widely expressed in epithelial and non-epithelial cells. Nature 1992;356:57-60.

van der Knaap MS et al. Leukoencephalopathy with swelling and a discrepantly mild clinical course in eight children. Ann Neurol 1995;37:324-334.

van der Knaap MS et al. Histopathology of an infantile-onset spongiform leukoencephalopathy with a discrepantly mild clinical course. Acta Neuropathol 1996;92:206-212.

van der Knaap MS et al. Defining and categorizing leukoencephalopathies of unknown origin: MR imaging approach. Radiology 1999;213:121-133.

van der Knaap MS et al. Megalencephalic leukoencephalopathy with cysts without MLC1 defect. Ann Neurol 2010;67:834-837.

van der Knaap MS et al. Megalencephalic leukoencephalopathy with subcortical cysts: chronic white matter oedema due to a defect in brain ion and water homoeostasis. Lancet Neurol 2012;11:973-985.

van der Voorn JP et al. Childhood white matter disorders: quantitative MR imaging and spectroscopy. Radiology 2006;241:510-517.

Appendix

Supplementary methods

Exome sequencing and Sanger sequencing

The exonic regions of the genome of the three patients with adult-onset disease were sequenced by DNAvision (Charleroi, Belgium). Genomic DNA was captured using the SureSelect Human All Exon 50 Mb kit (Agilent), followed by 75 base pair paired-end massively parallel sequencing on a HiSeq2000 sequencing system (Illumina), according to the manufacturers' instruction and protocols. Reads were mapped onto the reference genome (hg19) using the Burrows-Wheeler Aligner software (Li & Durbin, 2009; Li et al., 2009). Removing of duplicated reads and mutation calling were performed using samtools (Li & Durbin, 2009; Li et al., 2009) according to the following criteria: position coverage greater or equal to 20, mutation proportion greater or equal to 25%, and mutated bases called at least 10% on each strand.

The analysis of exome data assumed an autosomal recessive inheritance and was first based on the search for homozygous mutations located in identical-by-descent regions in patient 3. Possibly deleterious variants (i.e. with possible impact on gene or protein function) were defined as indels introducing frameshifts or in-frame insertions / deletions, nonsense or splice site mutations, mutations altering start or termination codons, or missense variants predicted at least once *in silico* to be deleterious and absent or not validated in control databases. Genes with at least one homozygous variant or at least two least two heterozygous variants predicted deleterious were listed for the three adult patients. The final analysis excluded possibly deleterious variants also detected in 7 exomes of individuals with other diseases performed at the same time to exclude false-positives and frequent variants not reported in databases.

The exons and intron-exon junctions of *CLCN2* (accession number NG_016422.1) were amplified and analyzed in these three adult patients, as described (Saint-Martin et al., 2009). In the four selected patients with pediatric-onset disease, the exons and intron-exon junctions of *CLCN2* were also sequenced, as described (Scheper et al., 2010). Primer sets were designed to amplify exons for the longest transcript variant (accession number NM_004366.4) with Primer3 (http://frodo.wi.mit.edu/primer3/). They are listed in Table S8. In those pediatric patients in whom no mutations were found or only one, *CLCN2* mRNA was isolated

from lymphoblasts and reverse-transcribed. *CLCN2* cDNA was amplified in four overlapping fragments, which were sequenced using primers listed in Table S6.

In the fourth patient, who had the X-linked disease the exons and intron-exon junctions of *GJB1* (accession number NG_008357.1) were amplified and analyzed (primers listed in Table S8).

Mutation interpretation was assessed using Alamut2.1 (Interactive Biosoftware), shown in Table S7. The *CLCN2* and *GJB1* mutation nomenclature is based on the cDNA reference sequences (NM_004366.4 and NM_000166.5 respectively), according to HGVS recommendations (www.hgvs.org/mutnomen).

Functional studies

CLCN2 mRNA was quantified in available fibroblasts of two adult patients with *CLCN2* mutations. Half of the cells were pretreated overnight with 10 µg/ml emetin to inhibit nonsense-mediated decay (NMD). Total RNA was isolated using the Qiagen RNeasy Mini kit (Invitrogen). First-strand synthesis was performed with 1 µg of total RNA using the SuperScript III First-Strand Kit (Invitrogen). Quantification was carried out using the Qiagen QuantiTect primer assays for *CLCN2*. *PPIA* and *GAPDH* were used as control genes. Each sample was run in triplicate on a Lightcycler-480 apparatus (Roche). Forty-five two-step cycles (30 s at 95°C and 30 s at 60°C) were performed. Analysis was performed using qbase Plus software (Biogazelle).

Cos7 cells were transiently co-transfected with 5 µg of ClC-2-V5-His6 expression plasmids[3] and pEYFP-Mem (Plasma membrane marker, Clontech) with a ratio 1:5, using a neon electroporation system (Invitrogen). For immunofluorescence staining, cells were fixed with 4% paraformaldehyde (PFA) 24h after transfection, permeabilized with 0.1% Triton X-100, and incubated with the primary antibody: monoclonal mouse anti-v5 (Abcam, ab27671, 1:10000), rabbit anti-ClC-2 (Sigma HPA024108, 1:200 or Santa Cruz SC-20122, 1:200), and/or anti-calreticulin (ER marker, Abcam, ab2907, 1:1000) for at least for 2 hours at room temperature. The signal was revealed by incubation with Alexa Fluor 488-coupled goat anti-rabbit or donkey anti-mouse IgG antibody (Invitrogen, 1:1000) or Cy3-coupled sheep anti-mouse or anti-rabbit IgG antibody (Sigma, 1:1000) for one hour at room temperature. Nuclei were stained with Hoescht (1:1000). Fluorescent images were acquired with a confocal system (Leica SP2 AOBS AOTF).

Proteins present at the plasma membrane were isolated following surface biotinylation on living Cos7 cells with the Cell Surface Protein Isolation Kit (Pierce),

following the manufacturer's recommendations. Proteins were resolved by SDS-PAGE on 4–12% gradient gels (Invitrogen) and electrotransferred onto nitrocellulose membranes. ClC-2 was probed with anti-v5 or anti-ClC-2 antibodies and the signal was revealed by enhanced chemiluminescence (Pierce). The membranes were then probed with anti-Flotillin-1 (BD Biosciences 610820) antibody for normalization. The ImageJ program (http://rsb.info.nih.gov/ij/) was used for signal quantification and calculation of Pearson Coefficients. For mRNA quantification and biotinylation assay, independent measures from at least three different experiments were compared with the Mann-Whitney test.

Western blot analyses of endogenous ClC-2 in human brain tissue

To study ClC-2 expression, three ClC-2 antibodies were used: GTX113403 (GeneTex), SC-20122 (Santa Cruz), and HPA24108 (Sigma). The GTX113403 and SC-20122 antibodies were both raised against the N-terminal part of ClC-2, whereas the HPA24108 antibody was raised against the C-terminal domain. To validate whether these anti-ClC-2 antibodies specifically detect ClC-2 in human brain samples, we performed several control experiments. First, HEK293 cells were transfected with the ClC-2-V5-His6 expression plasmid[3] using PEI.[5] Mock transfections were performed in parallel with pBlueScript. Lysates were prepared two days post-transfection as described (van Berge et al., 2013). Equal amounts of protein were applied to 11% SDS-PAGE without prior boiling, because boiling severely diminished ClC-2 detection with all tested antibodies (data not shown). The samples were subsequently transferred to Immobilon-P membrane (Millipore) overnight. Total protein loading was measured in-gel and on-blot with 2,2,2-trichloroethanol (TCE) that labels all tryptophans in the proteins (Ladner et al., 2004). TCE imaging was performed with Bio-Rad Image Lab software.

Membranes were blocked in 5% non-fat milk in PBS- 0.1% Tween and incubated overnight at 4˚C with primary antibody (1:1000 for GTX113403; 1:500 for SC-20122, 1:1000 for HPA24108 and 1:10000 for anti-v5). Subsequently, membranes were incubated with an HRP-conjugated secondary antibody (1:5000, Westburg) and further developed using the SuperSignal West Femto chemiluminescence-based detection kit (Pierce). Images were obtained with a Li-Cor Oddysey imager (Westburg) using the Image Studio software package.

We performed Western blot analyses with the same set of anti-ClC-2 antibodies on brain lysates prepared from two of the control individuals also investigated in fluorescent immunohistochemistry. Equal amounts of protein (~100 µg per well, as

determined by Bradford analysis) were applied to 4%-12% gradient gels without prior boiling (NuPAGE system, Invitrogen). After transfer, membranes were handled as described above. To increase the sensitivity of the assay, the blots were incubated with a goat anti-rabbit IgG secondary antibody (1 hr, 4˚C) and subsequently with an HRP-conjugated anti-goat IgG antibody (1 hr, 4˚C).

We also performed immunocytochemistry on the transfected HEK293 cells with the GTX113403 anti-ClC-2 antibody (1:200). The signal was detected with the AF488-conjugated anti-rabbit IgG antibody (Molecular Probes, 1:400).

Immunohistochemistry and electron microscopy

To study the expression of ClC-2, MLC1 and GlialCAM, tissue samples from the posterior limb of the internal capsule, frontal white matter, frontal cortex and ependymal lining were obtained at autopsy from 9 unrelated control subjects aged 1 to 75 years (7 males, 2 females), who succumbed to heart disease (lymphocytic myocarditis or acute myocardial infarction) or extra-cerebral tumor (gastric or bladder carcinoma). None of the subjects had neurological symptoms. Routine neuropathologic examination, including gross examination of the brain on cut and review of Hematoxylin and Eosin-stained tissue sections from multiple brain areas, was normal in all cases.

For light-microscopy purposes, 8-µm-thick frozen tissue sections were mounted on glass slides and fixed in 2% PFA, subsequently permeabilized with 0.1% saponin, blocked in 5% normal donkey serum and incubated with primary antibodies for 24 hours at 4°C. Immunohistochemistry was performed using antibodies against the following epitopes: glial fibrillary acidic protein (GFAP, Millipore, 1:1000); ClC-2 (GTX113403, 1:200; SC-20122, 1:20; HPA24108, 1:20); GlialCAM (R&D, 1:100); MLC1 (kind gift of Dr. R. Estévez, University of Barcelona, Spain, 1:100); oligodendrocyte transcription factor-2 (olig2, Millipore, 1:400); platelet endothelial cell adhesion molecule-1 (PECAM1/CD31, Dako, 1:50); neuronal nuclei (NeuN, Sigma, 1:500); phosphorylated neurofilaments (SMI31, Developmental Studies Hybridoma Bank, 1:1000); and non-phosphorylated neurofilament H (SMI32, Developmental Studies Hybridoma Bank, 1:1000). SMI31 and SMI32 antibodies were always applied simultaneously. In each experiment negative controls were included by omitting the primary antibody to verify the specificity of the immunohistochemical labeling. Specifically for the GTX113403 antibody, we included an isotype control rabbit IgG (SC-2027, Santa Cruz, 1:200). Furthermore, we performed a blocking experiment with this antibody. In brief, the protein (aa 27-

303 of ClC-2; GTX113403-PEP_SAMP, GeneTex) used to raise the GTX113403 antibody was pre-incubated with GTX113403 in a 100-fold molar excess for 2 hours at 4˚C whilst rotating. A control reaction was included in which the antigen was omitted.

After staining with secondary antibodies (Alexa 488-, 568-, and 594-tagged, Molecular Probes, 1:400), sections were counterstained with DAPI (Molecular Probes, 10 ng/ml) and photographed using a Leica DM6000B microscope (Leica Microsystems BV, Rijswijk, The Netherlands).

For electron microscopy (EM) purposes, tissue sections were fixed in 4% PFA, cryoprotected in 12.5% and 25% sucrose and frozen. Thirty to forty-µm-thick frozen sections were incubated for 96 hours with antibodies against ClC-2, GlialCAM, or MLC1, and then rinsed before being incubated in a PowerVisionPoly-HRP-Goat Anti-rabbit IgG or Anti-mouse IgG (ImmunoVision Technologies Co., Daly City, CA). To visualize the peroxidase, sections were incubated in a Tris-HCl diaminobenzidine (DAB) solution containing 0.03% H_2O_2. The DAB reaction product was then intensified by a gold-substituted silver peroxidase method (van den Pol & Gorcs, 1986). Sections were post-fixed for 20 minutes in 1% OsO4 supplemented with 1% in potassium ferricyanide in sodium cacodylate buffer 0.1 M (pH 7.4). The material was then dehydrated and embedded in epoxy resin. Ultrathin sections, longitudinal to the cortico-spinal tract, were examined and photographed with a FEI Technai 12 electron microscope.

All pictures were acquired as TIFF files. The images were optimized for brightness and contrast using Photoshop, version 7.0 (Abode systems, San Jose, CA).

Supplementary table 1. MRI findings

Patient	1	2	3	4	5	6	7
Age at MRI	63	59	47	14	11	10	15
MRI consistent with hypomyelination	-	-	-	+	+	+	+
Posterior fossa abnormalities							
medulla							
central tegmental tracts	-	-	-	+	+	+	-
pons							
pyramidal tracts	+	+	+	+	+	+	+
medial lemniscus	+	-	-	-	-	-	-
central tegmental tracts	+	+	-	+	+	+	-
midbrain							
cerebral peduncles	+	+	+	+	+	+	+
central tegmental tracts	+	+	+	+	+	+	-
decussation sup.cerebel.ped.	+	+	+	-	-	-	-
cerebellar peduncles							
superior	+	+	+	-	-	-	-
middle	+	+	+	+	+	+	+
inferior	-	-	-	-	-	-	-
cerebellar white matter	+	+	+	+	+, partial	+	+
Cerebral abnormalities							
posterior limb internal capsule	+	+	+	+	+	+	+
anterior limb internal capsule	slight	-	-	(-)**	(-)**	(-)**	(-)**
corpus callosum	slight	slight	slight	(-)**	-	(-)**	(-)**
hemispheric white matter	diffuse, slight	diffuse, slight	multifocal	(-)**	(-)**	(-)**	(-)**
Diffusion restriction*							
posterior limb internal capsule	+.	+	+	+	+***	+	+
cerebral peduncles	+.	+	-	+	+***	+	+
middle cerebellar peduncles	+	-	-	+	-	+	+

Supplementary table 1 (cont). MRI findings

Patient	1	2	3	4	5	6	7
Diffusion restriction*							
elsewhere	borderline-low in part of cerebral subcortical white matter	-	-	borderline-low in most cerebral and cerebellar hemispheric white matter and corpus callosum	borderline-low in part of cerebral white matter***	borderline-low in most cerebral hemispheric white matter and corpus callosum	borderline-low in most cerebral and cerebellar hemispheric white matter and corpus callosum

* low ADC ≤ 60 $10^{-5}mm^2/s$; borderline-low ADC between 50 and 60 $10^{-5}mm^2/s$. ** (-), signal consistent with lesion or hypomyelination. ***, printed films available only, showing diffusion restriction, but no quantitative measurements possible

Supplementary table 2. Coverage for targeted exome sequences for adult patients

	Patient 1	Patient 2	Patient 3*
Reads on target	60.13%	60.84%	60.41%
Reads on target ± 200	71.64%	72.57%	71.89%
Exon base coverage > 1	96.48%	96.99%	97.06%
Exon base coverage > 5	88.83%	89.79%	89.81%
Exon base coverage > 10	84.26%	85.39%	85.35%
Exon base coverage > 20	77.33%	78.29%	78.25%
Exon base coverage > 30	71.98%	72.44%	72.33%
Exon base coverage > 40	67.55%	67.46%	67.36%
Exon base coverage > 50	63.77%	63.20%	63.06%
Exon base coverage > 60	60.51%	59.46%	59.31%
Exon base coverage > 70	57.64%	56.12%	55.99%
Exon base coverage > 90	52.76%	50.26%	50.21%
Exon base coverage > 100	50.67%	47.64%	47.62%

*For patient 3 who has consanguineous parents, base coverage of homozygous regions exon was comprised between 75% and 93% with 84.4% of these regions being covered at least 20X.

Supplementary table 3. Statistics of the variants identified by exome sequence in adult patients

	Total number of variants	SNPs	Indels	Variants in the homozygous state	Nonsense variants	Frame-shifts	Missense variants
Patient 1	23117	21634	1483	8145	16	10	1190
Patient 2	24515	22937	1578	8880	10	14	1214
Patient 3	24234	22683	1551	9276	12	10	1327
Mean Number	23955	22418	1537	8767	13	11	1244

Supplementary table 4. Chromosomal coordinates (Hg18) of homozygous regions detected in patient 3 using Illumina cytoSNP-12 microarray

Chr	Start	End	Size
1	77 177 872	85766226	8 588 355
1	111 542 465	121 013 322	9 470 858
1	148 082 160	161 140 149	13 057 990
1	161 141 595	164 091 790	2 950 196
2	45 711 744	47 108 563	1 396 820
3	180 007 441	195 701 202	15 693 762
5	149 045 840	167 700 692	18 654 853
6	106 405 154	139 889 414	33 484 261
8	43 243 823	66 327 538	23 083 716
13	27 572 026	29 648 616	2 076 591
13	70 205 497	75 619 664	5 414 168
13	75 629 803	94 661 781	19 031 979
13	94 701 436	98 091 589	3 390 154
15	25 852 901	42 883 194	17 030 294
15	68 121 272	76 023 408	7 902 137
15	76 102 552	87 366 490	11 263 939
17	73 051 214	74 822 865	1 771 652
19	8 979 319	15 713 242	6 733 924
19	15 714 080	24 423 444	8 709 365
19	32 615 675	36 073 126	3 457 452
20	10 077 600	13 027 630	2 950 031
20	34 031 506	40 113 764	6 082 259
Total			**222 194 756**

Supplementary table 5. List of SNPs and indels that are absent or rare in databases (MAF < 1%), have a possible impact and are located in regions homozygous by descent in patient 3

Chr	Pos	Ref base	Mut base	Type	Zygosity	Gene	Impact	AA change	Rs number
1	160062119	G	A	point	hom	*IGSF8*	missense	A560V	NA
3	184587274	A	G	point	hom	*VPS8*	missense	Y18C	rs61741194
3	1184076015	T	-GATGAG	del	hom	*CLCN2*	in-frame	144: LITFSA →TFSA	NA
5	149907766	G	A	point	hom	*NDST1*	missense	R305H	NA
5	150563153	G	C	point	hom	*CCDC69*	missense	L246V	NA
6	128840288	T	G	point	hom	*PTPRK*	splice acceptor	NA	NA
13	29600208	G	A	point	hom	*MTUS2*	missense	R468Q	NA
15	42386638	C	A	point	hom	*PLA2G4D*	missense	G7V	NA
19	11305178	C	T	point	hom	*KANK2*	missense	V4I	NA
19	12258256	C	A	point	hom	*ZNF625*	missense	D49Y	NA
19	12258256	C	A	point	hom	*AC022415.5*	missense	D48Y	NA
20	11790885	C	+TT	ins	hom	*C20orf61*	frameshift	103: SM → KV*	rs34383977

Supplementary table 6. Number of genes containing homozygous or compound heterozygous variants in the 3 adult patients

	Number of autosomal genes with novel homozygous possibly deleterious variants	***Number of autosomal genes with at least two novel heterozygous and possibly deleterious variants***	***Number of autosomal genes with novel homozygous or at least two heterozygous, possibly deleterious variants***
Patient 1	32	19	53
Patient 2	30	18	37
Patient 3	37	22	42
Number of genes common to ≥ 2 patients	14	8	24
Number of genes common to the 3 patients	5	5	11*
Number of genes common to the 3 patients considering only variants absent from exomes of patients with other diseases**			**1 (*CLCN2*)**

* List of the 11 genes containing homozygous or at least two heterozygous, possibly deleterious variants common to the 3 adult patients: ***CLCN2***, *EXOC6B, KRTAP5-11, MPV17, MUC4, SENP3, SLC30A10, TAS2R43, TMPRSS13, ZNF717* and *ZNF880*.

** Most variants in the *EXOC6B, KRTAP5-11, MPV17, MUC4, SENP3, SLC30A10, TAS2R43, TMPRSS13,* ZNF717 and *ZNF880* genes were identical in all three adult patients and were also present in exome data from individuals with other diseases analyzed at the same time (n=7). *MUC4 and* ZNF717 harboured multiple variants in all affected individuals and controls.

Supplementary table 7. Pathogenicity prediction for *CLCN2* and *GJB1* mutations

		Conservation (a)		Align-GVGD (b)	Polyphen (c)	SIFT (d)	RNA (e)
Mutation	**effect**	**nucleotide**	**amino acid**				
***CLCN2* (f)**							
c.64-1107_639del, p.Met22Leufs*5	out frame deletion, premature stop codon						NMD
c.430_435del (g), p.Leu144_Ile145del	in frame deletion		up to *C. elegans*				
c.828dupG, p.Arg277Alafs*23	frameshift						NMD
c.1143delT, p.Gly382Alafs*34	frameshift						NMD
c.1499C>T, p.Ala500Val	missense	high (1.00)	up to *C. elegans*	C65	0.986	0.00	no effect
c.1709G>A, p.Trp570*(g)	premature stop codon						NMD
GJB1							
c.520C>T, p.Pro174Ser	missense	high (1.00)	up to fugu	C65	1.000	0.00	inconsistent

NMD, nonsense mediated decay. (a) conservation was analyzed in 14 species for *CLCN2*, including human, chimp, orangutan, macaque, rat, mouse, dog, cat, cow, opossum, frog, tetraodon, fruitfly and *C. elegans*; in 15 species for *GJB1*, including human, chimp, macaque, rat, mouse, dog, cat, cow, armadillo, opossum, platypus, chicken, frog, tetraodon and fugu. (b) C65 indicates most. (c) 0 (benign) - 1 (damaging). (d) [0.00-0.05] deleterious, [0.05-1.00] tolerated. (e) RNA splicing prediction programs in the Alamut software include SpliceSiteFinder-like, MaxEntScan, NNSPLICE, Human Splicing Finder. (f) *CLCN2* reference sequence NM_004366.4, GJB1 NM_000166.5; none of the mutations is reported in the 1000 genomes and HapMap databases (www.1000genomes.org and www.hapmap.org). (g) not found in 180 locally available healthy controls, matched for ethnicity likely to interfere with function, C0 most unlikely.

Supplementary table 8. Oligonucleotides for *CLCN2* and *GJB1* sequencing

Primer name*	Sequence (5' → 3')
CLCN2-1Fa	CTCCACGTGCCAGTAGACC
CLCN2-1Ra	GGGAAGGACACCTGAGACAA
CLCN2-2+3F	CTGGGAGAAGAGGAGTGGAG
CLCN2-2+3R	AGAAGCCAAGACGCCTTCC
CLCN2-4F	ACAGCCTGTCGTATCAGCG
CLCN2-4R	AGCCTGGAGGGAACAGTC
CLCN2-5F	CCTCAGGCTGTCGGTATGTT
CLCN2-5R	AAGAGGGAGAGGAACTTGCTG
CLCN2-6F	ATGAAGGAGTCCCTCCTGGT
CLCN2-6R	CATTCTGGCGAGAGTGGTG
CLCN2-7F	AACCCTGGGGCAAGTAGG
CLCN2-7R	CTAAGGCCTCAGACCCAGAT
CLCN2-8+9+10F	CCTTGGCCTCTCCTCCTTG
CLCN2-8+9+10R	TTTGACTGGGCCATTCTCTC
CLCN2-11+12F	GAGCCAAGGCTCTGCTCTG
CLCN2-11+12R	GAGAGGCTTCGAGGAGTGAG
CLCN2-13F	TAGACTTCTCCTGGGTGGC
CLCN2-13R	GGTGGGAAGAGAAAGAGGC
CLCN2-14F	GTGAGTTCTCAGCTGCCT
CLCN2-14R	GGACAGTCACACTCAGTCTC
CLCN2-15F	AGGGACCCACTCAGGACC
CLCN2-15R	GACCTTGCTAGAGGTGGCTG
CLCN2-16F	TGGAGCCCTCCTTGTGG
CLCN2-16R	CAAGGAGACTGGTCCTGAGC
CLCN2-17Fb	GCTCAGGACCAGTCTCCTTG
CLCN2-17Rb	CTTGAGTGCAGGCTTTAGGG
CLCN2-18+19F	GCAGGGTTATGACGTGGTC
CLCN2-18+19R	CTTCCAGGTGAGGGGAAAAG
CLCN2-20+21+22F	CACTGGCCTGAGTCCAAAC
CLCN2-20+21+22R	CTCCACCACTTCCCCTCAC
CLCN2-23Fb	CAGCAGTCCTGTCTCCTTCC
CLCN2-23Rb	ACCTCAGTGGTCTCCGTGTC
CLCN2-24Fb	AAGGAGGTGAGGTGATGGTG
CLCN2-24Rb	GCCTCTGGAAGACTTGTTGC

Supplementary table 8 (cont.). Oligonucleotides for *CLCN2* and *GJB1* sequencing

Primer name*	Sequence (5' → 3')
cCLCN2-1F	AGCCGAGTCCAGGACAGAG
cCLCN2-1R	AGAGGACGCCTCCAATAGGT
cCLCN2-2F	GCATCCCTGAGATGAAGACC
cCLCN2-2R	TAGGTGCTGCTGTCCGTATG
cCLCN2-3F	TGGTGGAGGAGCTAGAACCA
cCLCN2-3R	TGCTGGGAAGGCTGAGTC
cCLCN2-4F	ACAGGTGGTGGCATTGTTG
cCLCN2-4R	GCATGGCTAGCACCATCCTA
GJB1-1F	GAAAGACATGACCATCCTTCC
GJB1-1R	CGGATGATGAGGTACACCAC
GJB1-2F	GAAGAGGCACAAGGTCCA
GJB1-2R	GGAGGAAGGGAAGTAGCCA

* F forward, R reverse

Supplementary figure 1. Pedigrees

Adult patients

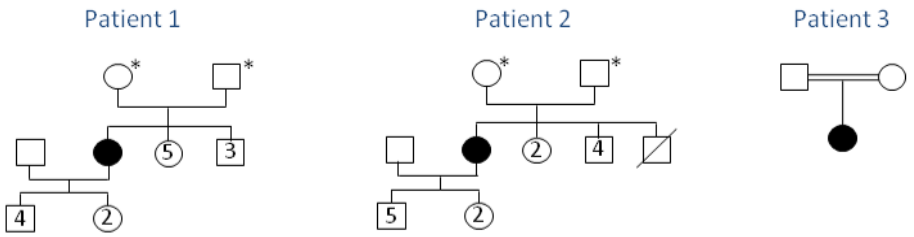

* No known consanguinity but parents come from the same small village

CMTX family

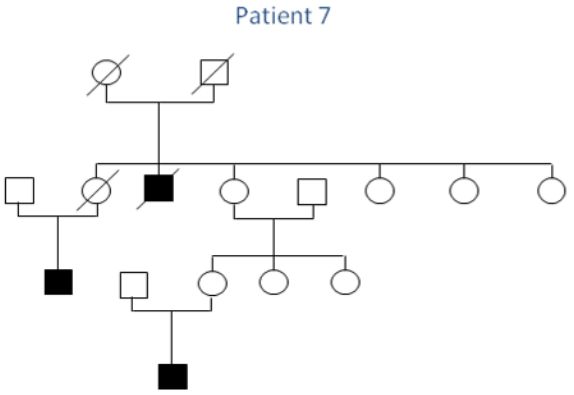

Supplementary figure 2. Confirmation of *CLCN2* mutations by Sanger sequencing and conservation of altered amino acids

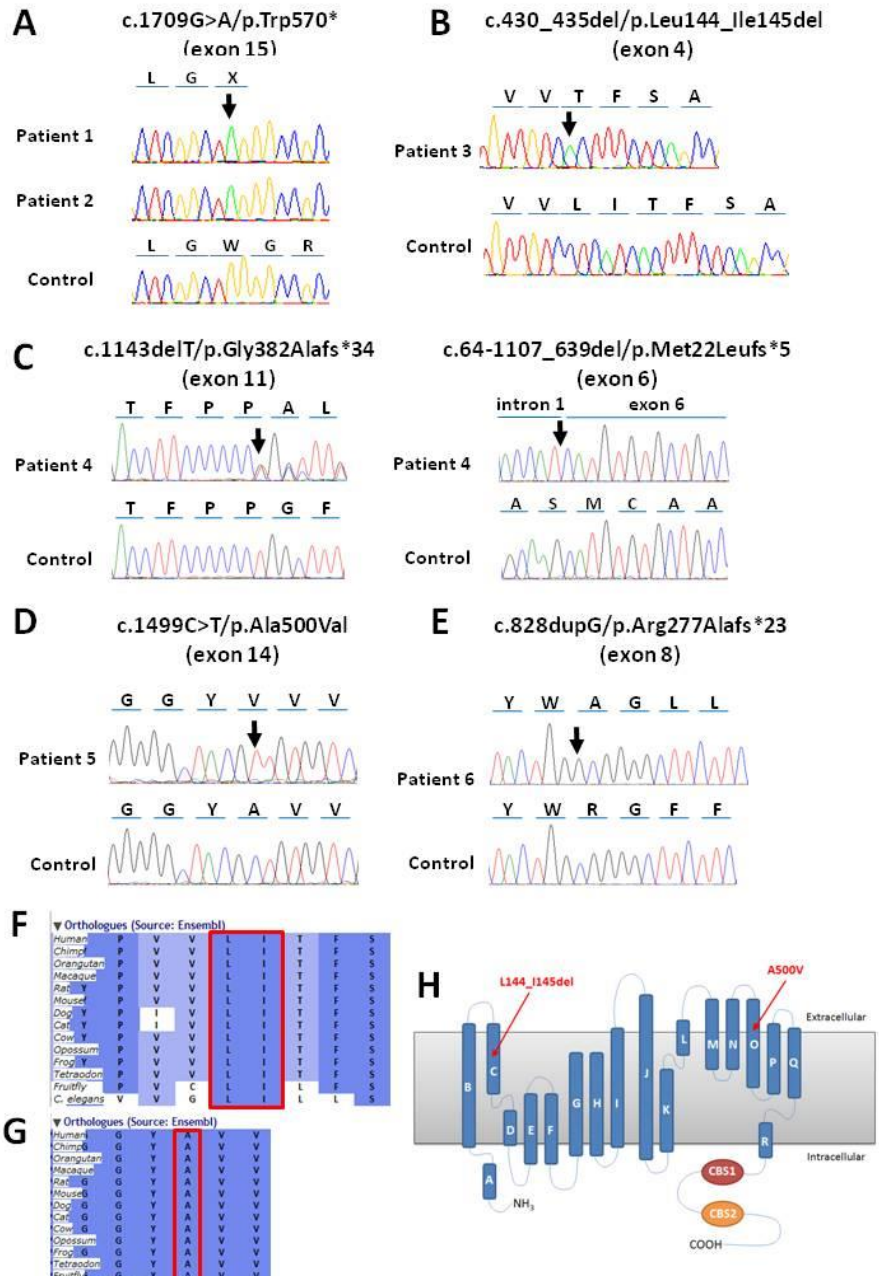

Supplementary figure 3. Quantification of *CLCN2* mRNA expression by real-time PCR

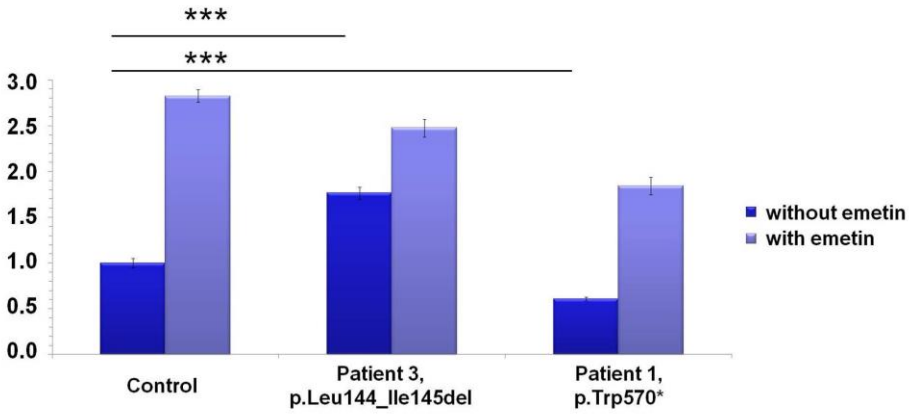

Quantification of CLCN2 expression in fibroblasts of patients 1 and 3 by real-time PCR showing that the Trp570* nonsense mutation specifically leads to CLCN2 mRNA down-regulation by nonsense-mediated decay (NMD), contrary to the Leu144_Ile 145 mutation. Treatment by emetin, a NMD-inhibitor, partially rescues mRNA expression although it also increases the mRNA levels in control individuals and in the patient with the Leu144_Ile 145 mutation. This result is compatible with the existence of many CLCN2 isoforms, some of which introducing premature termination codons (Scheper et al., 2010). PPIA and GAPDH were used as control genes for normalization. Values were compared with the Mann-Whitney test; ***: $p < 0.001$.

Supplementary figure 2. Sequence electropherograms of the c.1709G>A/p.Trp570* (A, patients 1 and 2), c430_435del/p.Leu144_Ile145del (B, patient 3), c.1143delT/p.Gly382AlafsX34 and c.64-1107_639del/p.Met22LeufsX5 (C, patient 4), c.1499C>T/p.Ala500Val (D, patient 5) and c.828dupG/p.Arg277AlafsX23 (E, patient 6) mutations in CLCN2. Mutation nomenclature is based on the CLCN2 transcript reference NM_004366. Nucleotides are numbered according to the cDNA with +1 corresponding to the A of the ATG translation initiation codon in the reference sequence. Orthologous protein alignments show that Leu144 and Ile145 (F) and Ala500 (G) are highly conserved during evolution (up to C. elegans). (H) Schematic representation of the ClC-2 channel showing the location of the p.Leu144_Ile145del and p.Ala500Val mutations in transmembrane domains of the ClC-2 protein. The topology of the ClC channel is based on a high resolution X-ray diffraction study of a ClC from Salmonella typhimurium (Dutzler et al., 2002).

Supplementary figure 4. Aberrant cellular localization of the c.1709G>A, p.Trp570* mutation

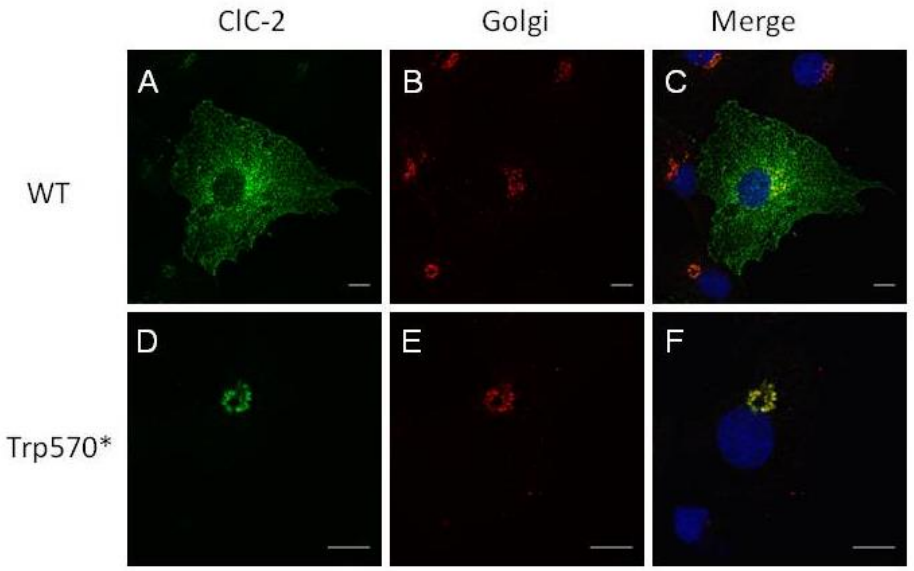

Subcellular localization of wild-type (A,C) and mutated (p.Trp570*, D,F) ClC-2 proteins, showing aberrant localization of the mutated protein in the Golgi apparatus (stained with anti-GM130, BD Biosciences 610822, 1:100, B, E). Cos7 cells were transiently transfected with wild-type or normal ClC-2-V5-His6 expression plasmid, fixed and permeabilized before staining with anti-ClC-2 (Santa Cruz SC-20122, 1:200), and examined by confocal microscopy. Scale bar: 10 µm.

Supplementary figure 5. Validation of anti-ClC-2 antibodies in Western blot analyses

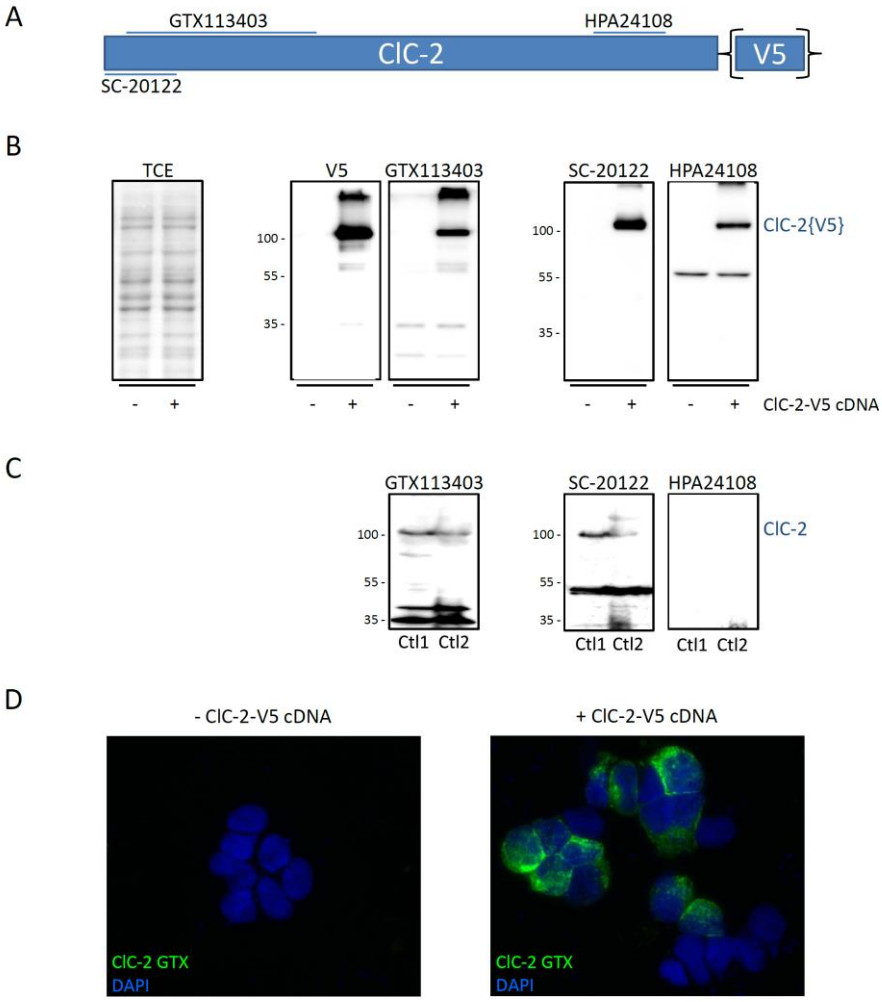

A shows the localization of the antigenic peptides that were used to raise the anti-ClC-2 antibodies. B shows Western blots of HEK293 cells after transfection with ClC-2-V5 expressing plasmids (+) or negative control (-). TCE stainings were performed to show that equal amounts of proteins were loaded. The antibodies used are indicated. C shows ClC-2 detection in control brain lysates. Only GTX113403 and SC-20122 detect a protein that migrates at the size expected for ClC-2. D shows immunocytochemistry of HEK293 cells after transfection with ClC-2-V5 expressing plasmids (+) and the negative control (-). ClC-2 was detected with the GTX113403 antibody (green). Nuclei are stained with DAPI (blue). Original magnifications: 400x.

Supplementary figure 6. Validation of the ClC-2 antibodies in fluorescent immunohistochemistry

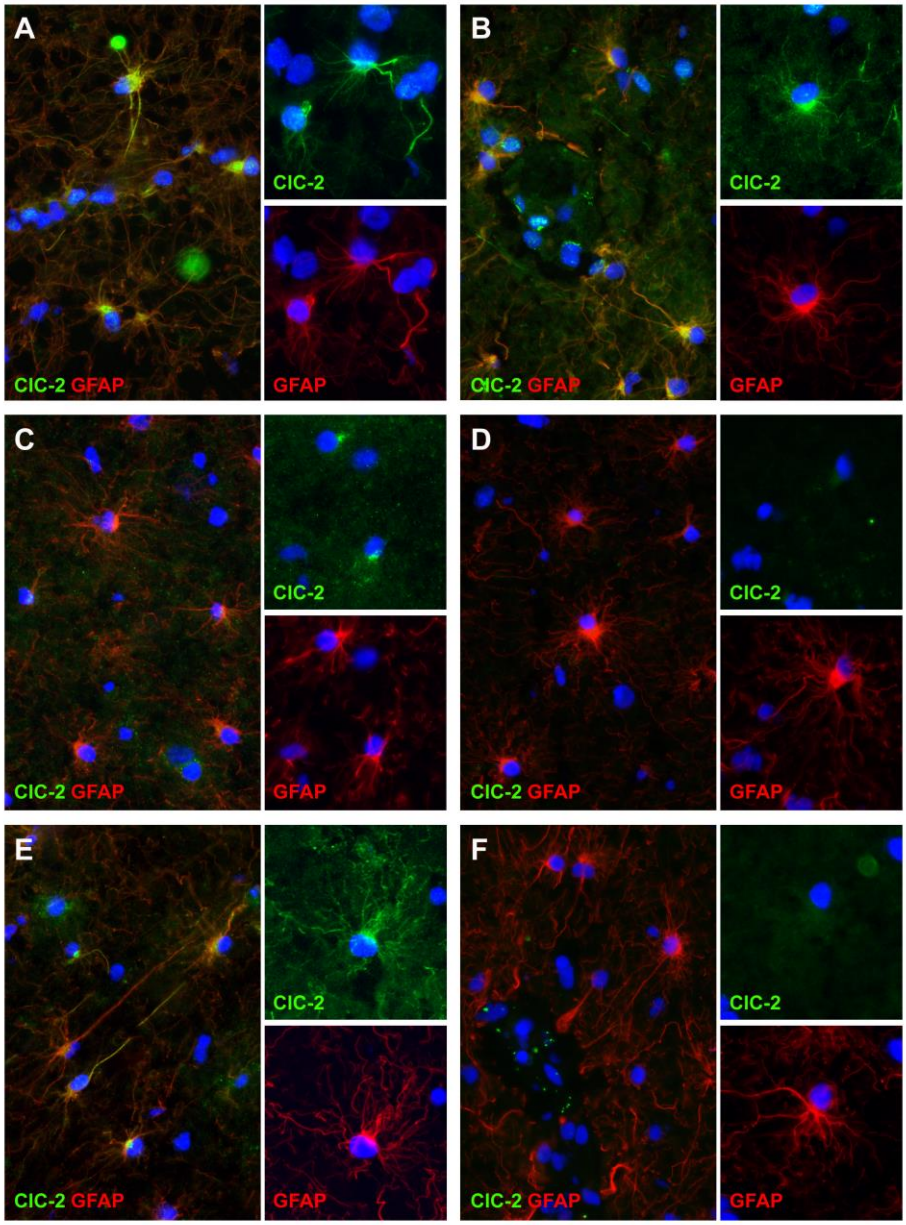

Anti-ClC-2 antibodies GTX113403 (A) and SC-20122 (B) show immunoreactivity (green) in GFAP$^+$ astrocytic processes (red) in the brain, whereas HPA24108 (C) does not. A normal rabbit IgG isotype control (D) does not show immunoreactivity in astrocytes either. E and F show a blocking experiment in which the GTX113403 antibody was pre-incubated with its antigen (F) or only serum (E). Nuclei are stained with DAPI (blue). Original agnifications: 400x.

Supplementary figure 7. ClC-2 localization in axons

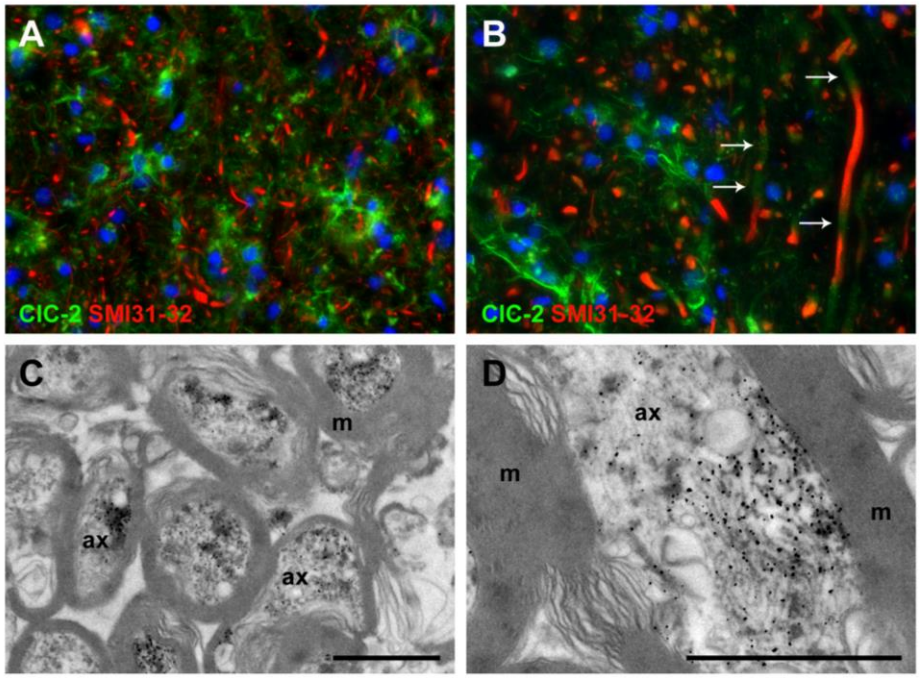

Double staining for ClC-2 (green) and the axonal markers SMI31-32 (red) of the posterior limb of the internal capsule shows numerous ClC-2^{+} astrocytes with processes abutting the surrounding axons (A, B). A fine punctate immunoreactivity is also present along the axons of larger caliber (arrows in B). Nuclei are stained with DAPI (blue). EM (C and D) confirms the presence of ClC-2 inside axons (C), associated with cytoskeletal elements and organelles, and lining the adaxonal surface of the myelin sheath (D). ClC-2 has a dynamic expression on the plasma membrane; rapid recycling and internalization could account for the abundant presence of ClC-2 in intracellular structures (Cornejo et al., 2009). Original magnifications (A, B): 400x; scale bars (C, D): 1 μm; ax: axons; m: myelin.

Supplementary figure 8. ClC-2, GlialCAM and MLC1 at blood-brain and cerebrospinal fluid-brain barriers

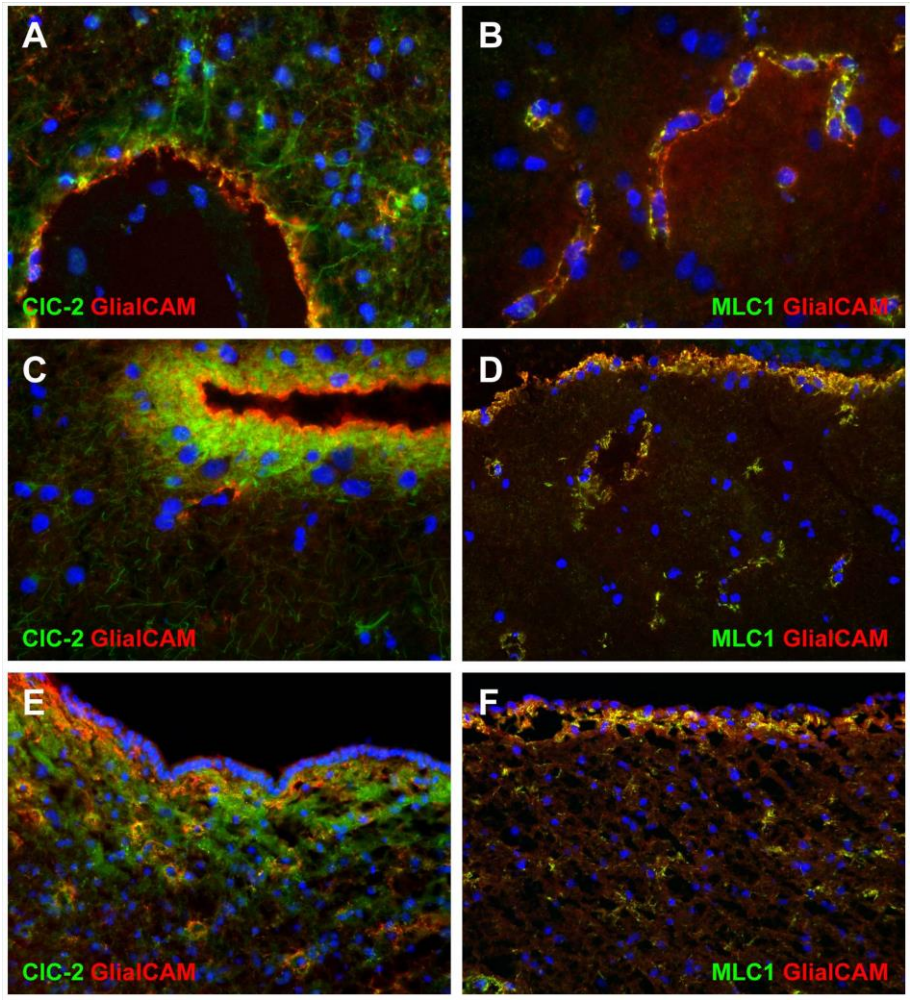

Double-labeling for ClC-2 and GlialCAM shows enhanced expression of ClC-2 (green) in astrocytes surrounding the blood vessels (A) and lining the surface of the brain (C) and the lateral ventricles (E). These astroycytes co-express GlialCAM (red) in the more distal portion of their cell processes and endfeet. Double staining for MLC1 (green) and GlialCAM (red) shows complete co-localization of the two proteins in the end feet of perivascular astrocytes (B), the subpial astrocytes (D), and in the ependymal cells (F). Nuclei are stained with DAPI (blue). Original magnifications: (A - C) 400x; (D - F) 200x.

Supplementary figure 9. Schematic view of action potential-driven potassium and water fluxes

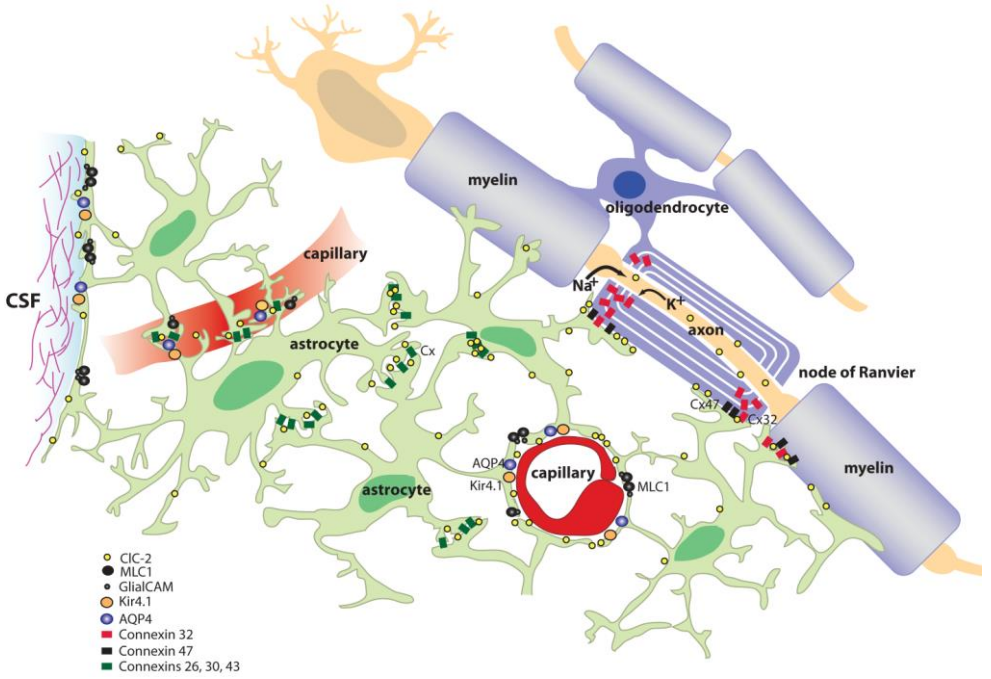

With each depolarization, sodium ions (Na^+) enter the axon at nodes of Ranvier. The compensatory exit of potassium ions (K^+) occurs at the paranodal axonal plasma membrane. K^+ and water pass through successive layers of myelin and enter the astrocytic syncytium via gap junctions, constituted by connexin32 (Cx32) and connexin47 (Cx47). The locations of ClC-2, MLC1, GlialCAM, the water channel aquaporin-4 (AQP4), the potassium channel Kir4.1 and the connexins are indicated by their respective symbols. Drawing by Dr. G.C. Scheper, modified from Rash (2010) and van der Knaap (2012) with permission.

Supplementary references

Cornejo I et al. Rapid recycling of ClC-2 chloride channels between plasma membrane and endosomes: role of a tyrosine endocytosis motif in surface retrieval. J Cell Physiol 2009;221:650-7.

Dutzler R et al. X-ray structure of a ClC chloride channel at 3.0 A reveals the molecular basis of anion selectivity. Nature 2002;415:287-94.

Ladner CL et al. Visible fluorescent detection of proteins in polyacrylamide gels without staining. Anal Biochem 2004;326:13-20.

Li H, Durbin R. Fast and accurate short read alignment with Burrows-Wheeler transform. Bioinformatics 2009;25:1754-60.

Li H et al. The Sequence Alignment/Map format and SAMtools. Bioinformatics 2009;25:2078-9.

Rash JE. Molecular disruptions of the panglial syncytium block potassium siphoning and axonal saltatory conduction: pertinence to neuromyelitis optica and other demyelinating diseases of the central nervous system. Neuroscience 2010;168:982-1008.

Saint-Martin C et al. Two novel CLCN2 mutations accelerating chloride channel deactivation are associated with idiopathic generalized epilepsy. Hum Mutat 2009;30:397-405.

Scheper GC et al. Analysis of CLCN2 as candidate gene for megalencephalic leukoencephalopathy with subcortical cysts. Genet Test Mol Biomarkers 2010;14:255-7.

van Berge L et al. Pathogenic mutations causing LBSL affect mitochondrial aspartyl-tRNA synthetase in diverse ways. Biochem J 2013;450:345-50.

van den Pol AN & Gorcs T. Synaptic relationships between neurons containing vasopressin, gastrin-releasing peptide, vasoactive intestinal polypeptide, and glutamate decarboxylase immunoreactivity in the suprachiasmatic nucleus: dual ultrastructural immunocytochemistry with gold-substituted silver peroxidase. J Comp Neurol 1986;252:507-21.

van der Knaap MS et al. Megalencephalic leukoencephalopathy with subcortical cysts: chronic white matter oedema due to a defect in brain ion and water homoeostasis. Lancet Neurol 2012;11:973-85.